Simulating Ion Trap Quantum Computers

Andrew Shaw[1, *]

[1] *University of Maryland, College Park, MD 20742, USA*

(Dated: October 12, 2022)

An ion trap quantum computer is simulated with an exponential speed-up using the *Stroboscopic Exponentiation Algorithm* (SEA).

I. PREFACE

Richard Feynman postulated the principle of *quantum supremacy*: *quantum computers* possess an innate computing advantage over *classical computers* [1].

A. Ion Trap Quantum Computing

Ion trap quantum computers (Figure 1) were proposed by *Ignacio Cirac* and *Peter Zoller* in May 1995 [2].

Ion trap quantum computers were experimentally demonstrated by *Christopher Monroe et al.* in December 1995 [3].

Ion trap quantum computers are the primary market competitors for *transmon quantum computers* [4–89].

1. Ion Trapping

An *ion trap* confines charged atoms to a spatial region using time-dependent electromagnetic fields [90–114].

2. Quantum Operations

Atomic qubits are pairs of *electronic states* associated with each ion (Figure 2) [115].

Lasers can induce transitions between the electronic states [116–143].

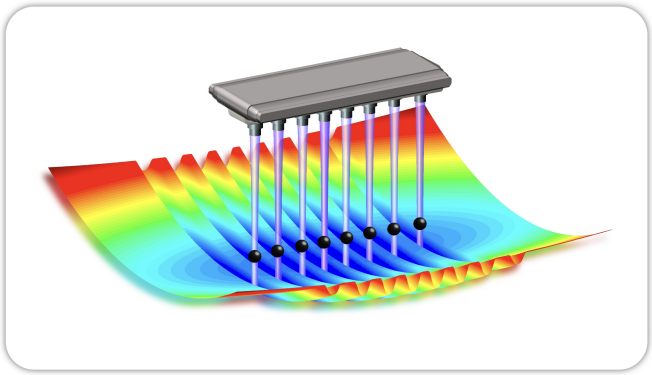

FIG. 1: An ion trap quantum computer is composed of ions (black) confined using electromagnetic fields (rainbow). The electronic states are manipulated using lasers (purple).

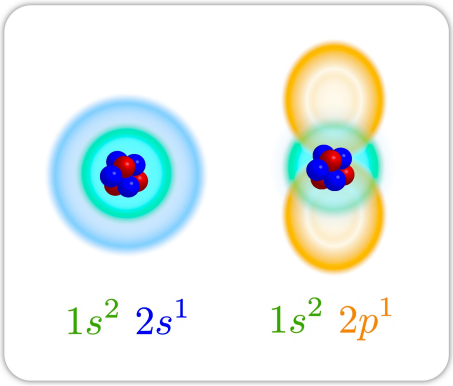

FIG. 2: An atomic qubit is composed of a spin-down (left) and spin-up (right) electronic state.

II. ION TRAP QUANTUM COMPUTERS

The *Hamiltonian* [144, 145] for an ion trap quantum computer is derived from quantum theory.

A. Ion Trap Hamiltonian

1. Ionic Hamiltonian

The ion trap parameters are the following:

$$\textit{Atomic Number}: \quad Z \tag{II.1}$$

$$\textit{Ion Charge}: \quad Qe \tag{II.2}$$

$$\textit{Ion Mass}: \quad M \tag{II.3}$$

$$\textit{Number of Ions}: \quad N \tag{II.4}$$

a. Kinetic Interactions

The *ionic kinetic energy operator* is the following [146]:

$$\hat{K}_{\text{ion}} = -\frac{1}{2M}\sum_{i=1}^{N}\hat{\vec{\nabla}}_i^2 \tag{II.5}$$

* Electronic Address: ashaw12@umd.edu

b. Ionic Interactions

The *ionic electrostatic operator* is the following [147]:

$$\hat{V}_{\text{elec}}^{(\text{ion})} = \frac{(Qe)^2}{8\pi} \sum_{\substack{i,j=1 \\ i \neq j}}^{N} \frac{1}{\left| \hat{\vec{x}}_i - \hat{\vec{x}}_j \right|} \tag{II.6}$$

c. Trapping Potential

The *trap electric field* is the following [91]:

$$\vec{E}_{\text{trap}}(\vec{x}, t) = \vec{E}_{\text{static}}(\vec{x}) + \vec{E}_{\text{dynamic}}(\vec{x}) \cos(\Omega_r t) \tag{II.7}$$

The *trap scalar potential* is the following [148]:

$$\phi_{\text{trap}}(\vec{x}, t) \approx -\int_{\vec{x}_r}^{\vec{x}} \vec{E}_{\text{trap}}(\vec{x}', t) \cdot d\vec{l}' \tag{II.8}$$

The *trapping operator* is the following:

$$\hat{V}_{\text{trap}}(t) = Qe \sum_{i=1}^{N} \hat{\phi}_{\text{trap}}(\vec{x}_i, t) \tag{II.9}$$

Over a timescale $t_{\text{trap}} \gg 1/\Omega_r$, the *trapping operator* can be approximated by a *confining operator* [149–151]:

$$\hat{V}_{\text{trap}}(t) \sim \hat{V}_{\text{confine}} \tag{II.10}$$

d. Ion-Laser Interaction

The *laser electric field* is the following:

$$\vec{E}_{\text{laser}}(\vec{x}, t) = \vec{E}_0(\vec{x})\, e^{i(\vec{k} \cdot \vec{x} - \omega t)} \tag{II.11}$$

The *laser magnetic vector potential* is given by the following [152]:[1]

$$\vec{\nabla}^2 \vec{A}_{\text{laser}}(\vec{x}, t) = -\frac{\partial \vec{E}_{\text{laser}}(\vec{x}, t)}{\partial t} \tag{II.12}$$

The *laser magnetic field* is the following:

$$\vec{B}_{\text{laser}}(\vec{x}, t) = \vec{\nabla} \times \vec{A}_{\text{laser}}(\vec{x}, t) \tag{II.13}$$

The *laser scalar potential* is the following:

$$\phi_{\text{laser}}(\vec{x}, t) = -\int_{\vec{x}_r}^{\vec{x}} \left[\vec{E}_{\text{laser}}(\vec{x}', t) + \frac{\partial \vec{A}_{\text{laser}}(\vec{x}', t)}{\partial t} \right] \cdot d\vec{l}' \tag{II.14}$$

The *ionic laser operator* is the following:

$$\begin{aligned} \hat{V}_{\text{laser}}^{(\text{ion})}(t) = &\sum_{i=1}^{N} \frac{iQe}{2M} \left(\hat{\vec{A}}_{\text{laser}}(\vec{x}_i, t) + h.c. \right) \cdot \hat{\vec{\nabla}}_i \\ &+ \frac{(Qe)^2}{8M} \left(\hat{\vec{A}}_{\text{laser}}(\vec{x}_i, t) + h.c. \right)^2 \\ &+ \frac{Qe}{2} \left(\hat{\phi}_{\text{laser}}(\vec{x}_i, t) + h.c. \right) \end{aligned} \tag{II.15}$$

e. Ionic Hamiltonian

The *ionic Hamiltonian* is the following:

$$\hat{H}_{\text{ion}}(t) = \hat{K}_{\text{ion}} + \hat{V}_{\text{elec}}^{(\text{ion})} + \hat{V}_{\text{confine}} + \hat{V}_{\text{laser}}^{(\text{ion})}(t) \tag{II.16}$$

2. Electronic Hamiltonian

a. Electron Number

The number of electrons in the trap is the following:

$$N_e = N(Z - Q) \tag{II.17}$$

b. Kinetic Term

The *electronic kinetic energy operator* is the following:

$$\hat{K}_{\text{e}} = -\frac{1}{2m_e} \sum_{r=1}^{N_e} \hat{\vec{\nabla}}_r^2 \tag{II.18}$$

c. Atomic Well

The *atomic well operator* is the following:

$$\hat{V}_{\text{atom}} = -\frac{Ze^2}{4\pi} \sum_{i=1}^{N} \sum_{r=1}^{N_e} \frac{1}{\left| \hat{\vec{x}}_i - \hat{\vec{y}}_r \right|} \tag{II.19}$$

[1] This relation holds in the *Coulomb gauge*: $\vec{\nabla} \cdot \vec{A} = 0$.

d. Electronic Interactions

The *electronic electrostatic operator* is the following:

$$\hat{V}^{(\mathrm{e})}_{\mathrm{elec}} = \frac{e^2}{8\pi} \sum_{\substack{r,s=1 \\ r\neq s}}^{N_e} \frac{1}{\left| \hat{\vec{y}}_r - \hat{\vec{y}}_s \right|} \tag{II.20}$$

e. Electron-Laser Interactions

The *electronic laser operator* is the following [153]:

$$\begin{aligned} \hat{V}^{(\mathrm{e})}_{\mathrm{laser}}(t) = &\sum_{r=1}^{N_e} \frac{e}{2im_e} \left(\hat{\vec{A}}_{\mathrm{laser}}(\vec{y}_r, t) + h.c. \right) \cdot \hat{\vec{\nabla}}_r \\ &+ \frac{e^2}{8m_e} \left(\hat{\vec{A}}_{\mathrm{laser}}(\vec{y}_r, t) + h.c. \right)^2 \\ &+ \frac{e}{4m_e} \hat{\vec{\sigma}}^{(s)}_r \cdot \left(\hat{\vec{B}}_{\mathrm{laser}}(\vec{y}_r, t) + h.c. \right) \\ &- \frac{e}{2} \left(\hat{\phi}_{\mathrm{laser}}(\vec{y}_r, t) + h.c. \right) \end{aligned}$$

f. Electronic Hamiltonian

The *electronic Hamiltonian* is the following:

$$\hat{H}_{\mathrm{electron}}(t) = \hat{K}_{\mathrm{e}} + \hat{V}_{\mathrm{atom}} + \hat{V}^{(\mathrm{e})}_{\mathrm{elec}} + \hat{V}^{(\mathrm{e})}_{\mathrm{laser}}(t) \tag{II.21}$$

3. Qubit Hamiltonian

a. Qubit States

The *atomic orbital Hamiltonian* for a single ion at $\vec{x}$ is the following [154]:

$$\hat{H}^{(\vec{x})}_{\mathrm{orbital}} = \sum_{r=1}^{N_e/N} \frac{\hat{\vec{p}}^{\,2}_r}{2m_e} - \frac{Ze^2}{4\pi \left| \vec{x} - \hat{\vec{y}}_r \right|} \tag{II.22}$$

The atomic orbital Hamiltonian's eigenstates form a complete basis centered at $\vec{x}$:

$$\hat{H}^{(\vec{x})}_{\mathrm{orbital}} \left| \alpha_{\mathrm{orbital}}(\vec{x}) \right\rangle = \lambda^{(\vec{x})}_{\alpha} \left| \alpha_{\mathrm{orbital}}(\vec{x}) \right\rangle \tag{II.23}$$

The *qubit states* are the following (Figure 2):

$$\left| \psi^{(\uparrow)}_q(\vec{x}) \right\rangle = \sum_{\alpha} c^{(\uparrow)}_{\alpha} \left| \alpha_{\mathrm{orbital}}(\vec{x}) \right\rangle \tag{II.24}$$

$$\left| \psi^{(\downarrow)}_q(\vec{x}) \right\rangle = \sum_{\alpha} c^{(\downarrow)}_{\alpha} \left| \alpha_{\mathrm{orbital}}(\vec{x}) \right\rangle \tag{II.25}$$

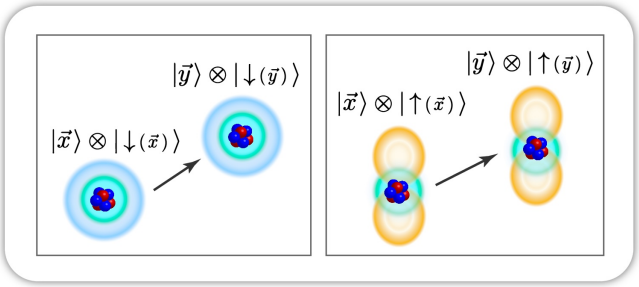

FIG. 3: The spin-down (left panel) and spin-up (right panel) qubit states vary with the ion position.

b. Passenger-Qubit Hilbert Space

The *passenger-qubit Hilbert space* at $\vec{x}$ is spanned by two states:

$$\mathcal{H}_q(\vec{x}) = \overline{\mathrm{span}} \left\{ \left| \vec{x} \right\rangle \otimes \left| \psi^{(\uparrow)}_q(\vec{x}) \right\rangle, \left| \vec{x} \right\rangle \otimes \left| \psi^{(\downarrow)}_q(\vec{x}) \right\rangle \right\} \tag{II.26}$$

In the passenger-qubit construction, the qubit states co-move with the ion (Figure 3).

c. Passenger-Qubit Basis States

In the multi-ion case, the *passenger-qubit basis states* are the following:

$$\begin{aligned} \left| \{\vec{x}_i\}, \vec{\alpha} \right\rangle = &\left| \vec{x}_1 \right\rangle \left| \vec{x}_2 \right\rangle \cdots \left| \vec{x}_N \right\rangle \\ &\otimes \left| \psi^{(\alpha_1)}_q(\vec{x}_1) \right\rangle \left| \psi^{(\alpha_2)}_q(\vec{x}_2) \right\rangle \cdots \left| \psi^{(\alpha_N)}_q(\vec{x}_N) \right\rangle \end{aligned} \tag{II.27}$$

d. Qubit Operators

Qubit operators are *projections* [155] of the electronic Hamiltonian into the passenger-qubit Hilbert space:[2]

$$\begin{aligned} \hat{\mathcal{P}}\left(\{\vec{x}_i\}, t\right) = \sum_{\vec{\alpha},\vec{\beta}} &\left\langle \{\vec{x}_i\}, \vec{\alpha} \right| \hat{H}_{\mathrm{electron}}(t) \left| \{\vec{x}_i\}, \vec{\beta} \right\rangle \\ &\left| \{\vec{x}_i\}, \vec{\alpha} \right\rangle \left\langle \{\vec{x}_i\}, \vec{\beta} \right| \end{aligned} \tag{II.28}$$

e. Pauli Decomposition

The *generalized Pauli operators* are the following [158, 159]:

$$\hat{\Sigma}\left(\vec{p}\right) = \hat{\sigma}_{p_1} \otimes \hat{\sigma}_{p_2} \otimes \cdots \hat{\sigma}_{p_N} \tag{II.29}$$

$$p_i \in \{0, 1, 2, 3\} \tag{II.30}$$

[2] To avoid an *effective Hamiltonian description* [156], a *passenger-qudit Hilbert space* is required for *hyperfine qubits* [157].

The qubit operators are decomposed in the *generalized Pauli basis* [160]:

$$\hat{\mathcal{P}}\big(\{\vec{x}_i\},t\big) = \sum_{\vec{p}} \mathcal{K}(\vec{p},t)\ \hat{\Sigma}(\vec{p}) \tag{II.31}$$

f. Qubit Hamiltonian

The *qubit Hamiltonian* is the following:

$$\hat{H}_{\text{qubit}}(t) = \left(\prod_{i=1}^{N}\int d^3x_i\right)\hat{\mathcal{P}}\big(\{\vec{x}_i\},t\big) \tag{II.32}$$

4. Ion Trap Hamiltonian

The *ion trap Hamiltonian* is the following:

$$\hat{H}_{\text{ion trap}}(t) = \hat{H}_{\text{ion}}(t) + \hat{H}_{\text{qubit}}(t) \tag{II.33}$$

B. Vibrational Expansion

The *vibrational expansion* [161, 162] approximates the near-equilibrium ion trap dynamics by collective oscillatory motion (Figure 4).

1. Vibrational Expansion

a. Total Ionic Potential Energy

In the absence of the laser, the ionic Hamiltonian is expressed using the *total ionic potential energy operator*:

$$\hat{H}_{\text{ion}} = \hat{K}_{\text{ion}} + \hat{V}_{\text{elec}}^{(\text{ion})} + \hat{V}_{\text{confine}} \tag{II.34}$$

$$= \hat{K}_{\text{ion}} + \hat{V}_{\text{total}} \tag{II.35}$$

b. Ionic Component Vector

The *ionic position components* are the following:

$$\vec{x}_i = \{x_i^{(1)}, x_i^{(2)}, x_i^{(3)}\} \tag{II.36}$$

They are used to form the *ionic component vector*:

$$\vec{c} = \left\{ x_1^{(1)}, x_1^{(2)}, x_1^{(3)}\,;\, x_2^{(1)}, x_2^{(2)}, x_2^{(3)}\,;\,\cdots\,;\, x_N^{(1)}, x_N^{(2)}, x_N^{(3)} \right\} \tag{II.37}$$

c. Component Gradient

The *component gradient* is the gradient with respect to the ionic component vector:

$$\vec{\nabla}_{\text{comp}} = \sum_{k=1}^{3N} \hat{\mathbf{c}}_{\mathbf{k}}\,\frac{\partial}{\partial c_k} \tag{II.38}$$

d. Critical Point

A *critical point* of the *total ionic potential energy* occurs at $\vec{c}_0$:

$$\vec{\nabla}_{\text{comp}} V_{\text{total}}(\vec{c})\Big|_{\vec{c}\,=\,\vec{c}_0} = \vec{0} \tag{II.39}$$

The vibrational expansion is made by expanding the total ionic potential energy around $\vec{c}_0$:

$$V_{\text{total}}(\vec{c})$$

$$= \sum_{n=0}^{\infty} \frac{1}{n!}\left(\vec{\nabla}_{\text{comp}}\right)^n_{\otimes_{\text{outer}}} V_{\text{total}}(\vec{c})\,\Big|_{\vec{c}\,=\,\vec{c}_0} \cdot \left(\vec{c}-\vec{c}_0\right)^n_{\otimes_{\text{outer}}} \tag{II.40}$$

$$= \sum_{n=0}^{\infty} \frac{1}{n!}\left(\vec{\nabla}_{\text{comp}}\right)^n_{\otimes_{\text{outer}}} V_{\text{total}}(\vec{c})\,\Big|_{\vec{c}\,=\,\vec{c}_0} \cdot \left(\vec{\Delta}c\right)^n_{\otimes_{\text{outer}}} \tag{II.41}$$

$$= \sum_{n=0}^{\infty} \mathcal{V}_n(\vec{c}) \tag{II.42}$$

e. Potential Hessian Matrix

The second-order contribution to the vibrational expansion is expressed as a matrix equation:

$$\mathcal{V}_2(\vec{c}) = (\vec{\Delta}c)^T\ \hat{\mathbf{A}}\ (\vec{\Delta}c) \tag{II.43}$$

$$= \sum_{m,n=1}^{3N} (\Delta c)_m\ \hat{\mathbf{A}}_{m,n}\ (\Delta c)_n \tag{II.44}$$

The *potential Hessian matrix* is the following [92]:

$$\hat{\mathbf{A}}_{a,b} = \frac{1}{2}\,\frac{\partial}{\partial c_a}\,\frac{\partial}{\partial c_b}\,V_{\text{total}}(\vec{c})\Big|_{\vec{c}\,=\,\vec{c}_0} \tag{II.45}$$

f. Trap Frequencies

The potential Hessian matrix is *diagonalized* as follows:

$$\hat{\mathbf{A}} = \hat{\mathbf{O}}^T \, \hat{\mathbf{D}} \, \hat{\mathbf{O}} \tag{II.46}$$

The eigenvalues of the potential Hessian matrix provide access to the *trap frequencies*:

$$\hat{\mathbf{D}}_{a,a} = \omega_a^2 \tag{II.47}$$

2. Ladder Hamiltonian

a. Vibrational Mode Vector

The *vibrational mode vector* is the following (Figure 4):

$$\vec{m} = \hat{\mathbf{O}} \, \vec{\Delta} c \tag{II.48}$$

$$m_a = \sum_{b=1}^{3N} \emptyset_{a,b} \, \left(c_b - c_{0,b} \right) \tag{II.49}$$

b. Harmonic Interactions

The second-order contribution to the vibrational expansion is written in harmonic form:

$$\mathcal{V}_2(\vec{c}) = \left(\vec{\Delta} c \right)^T \, \hat{\mathbf{O}}^T \, \hat{\mathbf{D}} \, \hat{\mathbf{O}} \, \left(\vec{\Delta} c \right) \tag{II.50}$$

$$= \left(\vec{m} \right)^T \, \hat{\mathbf{D}} \, \left(\vec{m} \right) \tag{II.51}$$

$$= \sum_{a=1}^{3N} \omega_a^2 \, m_a^2 \tag{II.52}$$

c. Component Laplacian

The *component Laplacian* is the following:

$$\vec{\nabla}^2_{\text{comp}} = \sum_{k=1}^{3N} \frac{\partial^2}{\partial c_k^2} \tag{II.53}$$

The first partial derivative is expressed in terms of the vibrational mode vector components (Equation II.49):

$$\frac{\partial}{\partial c_k} = \sum_{a=1}^{3N} \frac{\partial m_a}{\partial c_k} \frac{\partial}{\partial m_a} \tag{II.54}$$

$$= \sum_{a=1}^{3N} \emptyset_{a,k} \frac{\partial}{\partial m_a} \tag{II.55}$$

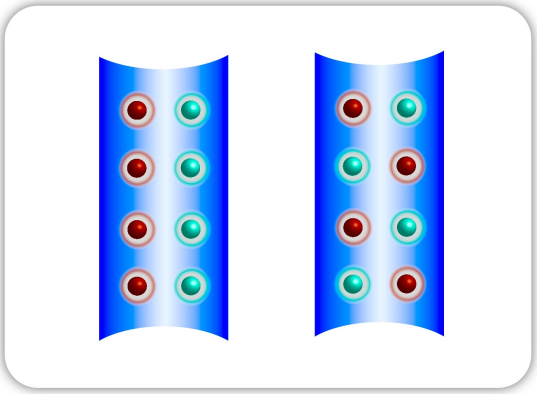

FIG. 4: The ions oscillate collectively (red ↔ green) in the ion trap (blue). The *center-of-mass mode* (left) and the *zig-zag mode* (right) are shown [156].

The component Laplacian is the following:

$$\vec{\nabla}^2_{\text{comp}} = \sum_{k=1}^{3N} \sum_{a,b=1}^{3N} \left(\emptyset_{a,k} \right) \left(\emptyset_{b,k} \right) \left(\frac{\partial^2}{\partial m_a \, \partial m_b} \right) \tag{II.56}$$

$$= \sum_{a,b=1}^{3N} \delta_{a,b} \, \frac{\partial^2}{\partial m_a \, \partial m_b} = \sum_{a=1}^{3N} \frac{\partial^2}{\partial m_a^2} \tag{II.57}$$

d. Kinetic Interactions

The ionic kinetic energy operator is the following:

$$\hat{K}_{\text{ion}} = -\frac{1}{2M} \sum_{k=1}^{3N} \frac{\partial^2}{\partial \hat{m}_k^2} \tag{II.58}$$

$$= \frac{1}{2M} \sum_{k=1}^{3N} \hat{p}_k^2 \tag{II.59}$$

e. Ionic Hamiltonian

The ionic Hamiltonian is the following:

$$\hat{H}_{\text{ion}} = \sum_{k=1}^{3N} \frac{\hat{p}_k^2}{2M} + \omega_k^2 \, \hat{m}_k^2 + \mathcal{O}\left(\left| \vec{\Delta} c \right|^3 \right) \tag{II.60}$$

f. Mode Ladder Operators

The *mode ladder operators* are the following [163]:

$$\hat{a}_k^\dagger = \left(\frac{M \omega_k^2}{2} \right)^{1/4} \hat{m}_k - i \left(\frac{1}{8 M \omega_k^2} \right)^{1/4} \hat{p}_k \tag{II.61}$$

$$\hat{a}_k = \left(\frac{M \omega_k^2}{2} \right)^{1/4} \hat{m}_k + i \left(\frac{1}{8 M \omega_k^2} \right)^{1/4} \hat{p}_k \tag{II.62}$$

g. Ladder Hamiltonian

The ionic Hamiltonian becomes the following, up to an overall constant:

$$\hat{H}_{\text{ion}} = \sqrt{\frac{2}{M}} \sum_{k=1}^{3N} \omega_k \left\{ \hat{a}_k^\dagger \, \hat{a}_k \right\} + \mathcal{O}\Big(\left| \vec{\Delta} c \right|^3 \Big) \tag{II.63}$$

The ionic Hamiltonian can be expressed in terms of the *physical trap frequencies* [164]:

$$\hat{H}_{\text{ion}} = \sum_{k=1}^{3N} \tilde{\omega}_k \left\{ \hat{a}_k^\dagger \, \hat{a}_k \right\} + \mathcal{O}\Big(\left| \vec{\Delta} c \right|^3 \Big) \tag{II.64}$$

C. Effective Ion Trap Hamiltonian

Effective approximations are used to tailor the ion trap Hamiltonian for quantum computing applications [165].

1. Strong–Confinement Approximation

The *strong-confinement approximation* (SCA) is the following (Figure 5):

$$\sum_{n=3}^{\infty} \left| \left\langle \hat{\mathcal{V}}(n) \right\rangle \right| \ll \left| \left\langle \hat{\mathcal{V}}(2) \right\rangle \right| \tag{II.65}$$

The *effective ionic Hamiltonian* is as follows:

$$\hat{H}_{\text{ion}}^{(\text{eff})} = \sum_{k=1}^{3N} \tilde{\omega}_k \left\{ \hat{a}_k^\dagger \, \hat{a}_k \right\} \tag{II.66}$$

2. Weak–Laser Approximation

The *weak-laser approximation* (WLA) is as follows (Figure 6):

$$\left| \left\langle \hat{V}_{\text{laser}}(t) \right\rangle \right| \ll \left| \left\langle \hat{H}_{\text{ion}} \right\rangle \right| \tag{II.67}$$

The *effective ion trap Hamiltonian* is the following:

$$\hat{H}_{\text{ion trap}}^{(\text{eff})}(t) = \sum_{k=1}^{3N} \tilde{\omega}_k \left\{ \hat{a}_k^\dagger \, \hat{a}_k \right\} + \hat{H}_{\text{qubit}}(t) \tag{II.68}$$

$$= \hat{H}_{\text{phonon}} + \hat{H}_{\text{qubit}}(t) \tag{II.69}$$

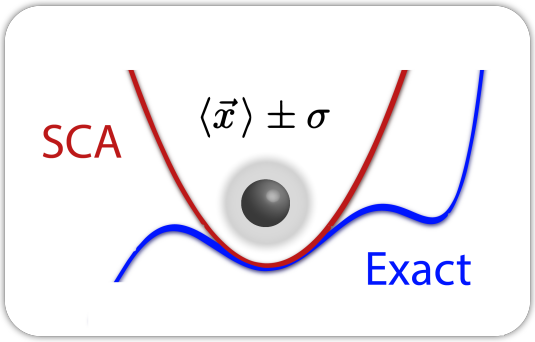

FIG. 5: If the ion (gray) is strongly confined, the total potential energy (blue) can be approximated (red).

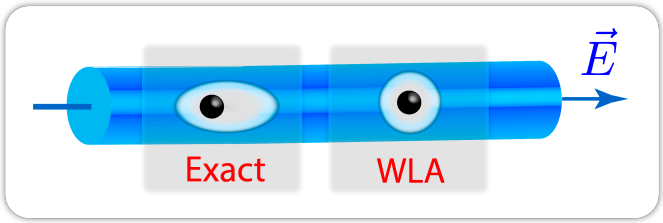

FIG. 6: If the laser (blue) is sufficiently weak, its effect on the ionic wavefunction (left) can be neglected (right).

D. Interaction Picture Hamiltonian

1. Interaction Picture

The *interaction picture* leverages the effective ionic Hamiltonian's analytic evolution operator for faster computation [166].

a. Interaction Picture Hamiltonian

The *effective interaction picture Hamiltonian* is the following:

$$\hat{H}_{\text{ion trap}}^{(\text{eff},I)}(t) = e^{\,i t \hat{H}_{\text{phonon}}} \;\; \hat{H}_{\text{qubit}}(t) \;\; e^{-i t \hat{H}_{\text{phonon}}} \tag{II.70}$$

2. Spin–Phonon Interactions

a. Phonon Passenger-Qubit Basis

The *phonon passenger-qubit basis states* are as follows:

$$\left| \vec{n}, \vec{\alpha} \right\rangle = \left| n_1 \right\rangle \left| n_2 \right\rangle \cdots \left| n_{3N} \right\rangle \otimes \left| \psi_q^{(\alpha_1)}(\vec{n}) \right\rangle \left| \psi_q^{(\alpha_2)}(\vec{n}) \right\rangle \cdots \left| \psi_q^{(\alpha_N)}(\vec{n}) \right\rangle \tag{II.71}$$

b. Spin-Phonon Operators

The *spin-phonon operators* are projections of the electronic Hamiltonian into the *phonon passenger-qubit Hilbert space*:

$$\hat{\mathcal{S}}^{(t)}_{\vec{n},\vec{m},\vec{\alpha},\vec{\beta}} = |\vec{n},\vec{\alpha}\rangle\langle\vec{n},\vec{\alpha}|\ \hat{H}_{\text{electron}}(t)\ |\vec{m},\vec{\beta}\rangle\langle\vec{m},\vec{\beta}| \quad \text{(II.72)}$$

The effective interaction picture Hamiltonian is written explicitly:

$$\hat{H}^{(\text{eff},I)}_{\text{ion trap}}(t) = \sum_{\vec{n},\vec{m},\vec{\alpha},\vec{\beta}} e^{\,it\sum_{k=1}^{3N}\tilde{\omega}_k(n_k-m_k)}\ \hat{\mathcal{S}}^{(t)}_{\vec{n},\vec{m},\vec{\alpha},\vec{\beta}} \quad \text{(II.73)}$$

III. CLASSICAL QUANTUM-SIMULATION ALGORITHMS

An algorithm is proposed to efficiently simulate ion trap quantum computers.

A. Product-Formula Algorithms

Product-formula algorithms (PFAs) [167] are a family of *quantum-simulation algorithms* [168].[3]

PFAs can be represented schematically in three stages:

I. Discretization: Subdivide the simulation time into sub-regions.

II. Piece-wise Simulation: Approximate the sub-region evolution operators.

III. Matrix Multiplication: Take the ordered product of the sub-region evolution operators.

1. Evolution Operator

a. Hamiltonian Operator

The Hamiltonian is the following:

$$\hat{H}_{\text{sim}}(t) = \sum_{\alpha=1}^{d} \mathcal{E}_\alpha(t)\ |\alpha(t)\rangle\langle\alpha(t)| \quad \text{(III.1)}$$

[3] The PFA is an extremely versatile algorithmic framework, with mathematical [169–193], low-energy [194–216], and high-energy [217–231] physics applications.

b. Time-Ordered Exponential

The *evolution operator* is the following:

$$\hat{U}_{\text{sim}}(t) = \mathcal{T}\left\{ e^{-i\int_0^t dt'\ \hat{H}_{\text{sim}}(t')} \right\} \quad \text{(III.2)}$$

2. Discretization

a. Sub-Regions

The *simulation time* τ is subdivided into L_{sim} *sub-regions*:

$$\delta t = \frac{\tau}{L_{\text{sim}}} \quad \text{(III.3)}$$

b. Sub-Region Evolution Operators

The *sub-region evolution operators* are the following:

$$\hat{U}^{(r)}_{\text{sub}} = \mathcal{T}\left\{ e^{-i\int_{(r-1)\,\delta t}^{r\,\delta t} dt'\ \hat{H}_{\text{sim}}(t')} \right\} \quad \text{(III.4)}$$

The evolution operator can be written as an *ordered-product* of the sub-region evolution operators:

$$\hat{U}_{\text{sim}}(t) = \prod_{\substack{r=1\\ \leftarrow}}^{L_{\text{sim}}} \hat{U}^{(r)}_{\text{sub}} \quad \text{(III.5)}$$

$$= \hat{U}^{(L_{\text{sim}})}_{\text{sub}} \cdots \hat{U}^{(2)}_{\text{sub}}\ \hat{U}^{(1)}_{\text{sub}} \quad \text{(III.6)}$$

3. Piece–Wise Simulation

An *intermediate simulation algorithm* is used to generate the *approximate sub-region evolution operators*:

$$\hat{U}^{(r)}_{a,\text{sub}} = \hat{U}^{(r)}_{\text{sub}} + \hat{\mathcal{E}}^{(r)}_{\text{sub}} \quad \text{(III.7)}$$

4. Matrix Multiplication

An ordered-product is used to generate the *approximate evolution operator*:

$$\hat{U}_{a,\text{sim}}(t) = \prod_{\substack{r=1\\ \leftarrow}}^{L_{\text{sim}}} \hat{U}^{(r)}_{a,\text{sub}} \quad \text{(III.8)}$$

B. Time-Integrated Product-Formula Algorithm

The *time-integrated product-formula algorithm* (TI-PFA) coarse-grains the Hamiltonian to minimize the number of required sub-regions [232–234].

1. Time–Integrated Product–Formula Algorithm

TI-PFA can be represented schematically in three stages:

I. Time-Averaging: Time-average the Hamiltonian over the sub-regions.

II. Matrix Exponentiation: Generate the approximate sub-region evolution operators.

III. Matrix Multiplication: Take the ordered product of the approximate sub-region evolution operators.

a. Time-Averaging

The *sub-region Hamiltonians* are as follows (Figure 7):

$$\hat{H}^{(r)}_{\text{sub}} = \frac{1}{\delta t}\int_{(r-1)\,\delta t}^{r\,\delta t} dt'\,\hat{H}_{\text{sim}}(t') \tag{III.9}$$

b. Matrix Exponentiation

The approximate sub-region evolution operators are the following:

$$\hat{U}^{(r)}_{a,\text{sub}} = e^{-i\,\delta t\,\hat{H}^{(r)}_{\text{sub}}} \tag{III.10}$$

c. Sub-Region Evolution Operator Error

The *eigenvalue spread* is as follows (Equation III.1):[4]

$$\mathcal{H} = \left|\max\Big\{\,\mathcal{E}_\alpha(t)\,\Big\} - \min\Big\{\,\mathcal{E}_\alpha(t)\,\Big\}\right|_{\overline{\max}\,\tau} \tag{III.11}$$

The *sub-region error coefficient* is the following:

$$E_{\text{sub}} = \mathcal{H}\,\delta t \tag{III.12}$$

The error in the sub-region evolution operator is given by the *Baker-Campbell-Hausdorff formula* [235]:

$$\hat{\mathcal{E}}^{(r)}_{\text{sub}} = 0 + \mathcal{O}\left(E^2_{\text{sub}}\right) \tag{III.13}$$

[4] The notation $\overline{\max}\,\tau$ indicates a maximum taken over time τ.

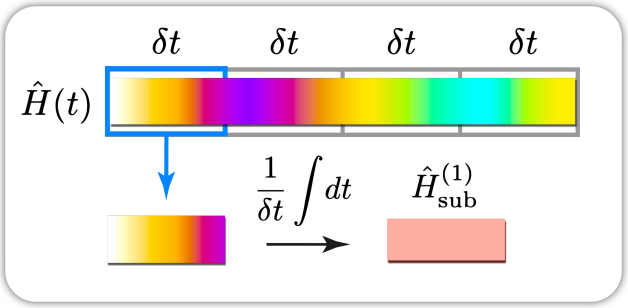

FIG. 7: The simulation time is discretized (top) and for each sub-region (blue) the Hamiltonian is time-averaged.

C. Quantum-Simulation Computational Cost

The *computational cost* of TI-PFA is determined by counting the number of *elementary operations* [236].

1. Matrix Exponentiation

The approximate sub-region evolution operators are computed using a Λ-*truncated Taylor series* [237]:

$$\hat{U}^{(r,\Lambda)}_{a,\text{sub}} = \sum_{n=0}^{\Lambda}\frac{\left(-i\,\hat{H}^{(r)}_{\text{sub}}\,\delta t\right)^n}{n!} \tag{III.14}$$

The number of matrix multiplications required for the computation is the following:

$$N_{\text{Mult}} = \left(\Lambda - 1\right) \tag{III.15}$$

2. Matrix Multiplication

Classical computers perform matrix multiplication by manipulating *matrix elements*:

$$\left(\mathbf{A}\times\mathbf{B}\right)_{i,j} = \sum_{k=1}^{d}\mathbf{A}_{i,k}\mathbf{B}_{k,j} \tag{III.16}$$

The number of elementary operations required in the *textbook matrix multiplication algorithm* is as follows [236]:

$$N_{\text{op.}} = d^3 \tag{III.17}$$

The *time-complexity* is the length of time required for a *computing algorithm* to run to completion [236]:

$$\mathcal{T}_c = t_{\text{op}}\,N_{\text{op}} \tag{III.18}$$

3. Computational Cost

a. Matrix Exponentiation Cost

The computational cost of approximating all of the sub-region evolution operators is the following:

$$\mathcal{T}_c\left\{\hat{U}_{a,\text{sub}}^{(r,\Lambda)}\right\} = \left(\Lambda - 1\right) L_{\text{sim}} \;\; t_{\text{op}}\; d^3 \tag{III.19}$$

b. Matrix Multiplication Cost

The computational cost of generating the ordered product is the following:

$$\mathcal{T}_c\left\{\text{Multiplication}\right\} = \left(L_{\text{sim}} - 1\right) t_{\text{op}}\; d^3 \tag{III.20}$$

c. Algorithm Cost

The computational cost of TI-PFA is the following:

$$\mathcal{T}_c\left\{\text{TI-PFA}\right\} = \left\{\; \Lambda\; L_{\text{sim}} - 1 \;\right\} t_{\text{op}}\; d^3 \tag{III.21}$$

4. Quantum–Simulation Error

a. Algorithm Error

The error in TI-PFA is the following (Equation III.13):

$$\epsilon_{\text{TI-PFA}} \sim L_{\text{sim}}\, \hat{\mathcal{E}}_{\text{sub}}^{(r)} \tag{III.22}$$

$$\epsilon_{\text{TI-PFA}} \sim \mathcal{H}\tau\;\; \mathcal{O}\big(E_{\text{sub}}\big) \tag{III.23}$$

If the *disretization condition* holds, TI-PFA will achieve the *target simulation error* reliably:

$$L_{\text{sim}} \gg \frac{\mathcal{H}^2\,\tau^2}{2\,\epsilon_{\text{target}}} + \frac{\mathcal{H}\tau}{2} \tag{III.24}$$

b. Minimum Algorithm Cost

The *perturbative noise condition* must hold for TI-PFA to converge (Equation III.13):

$$E_{\text{sub}} < 1 \tag{III.25}$$

The perturbative noise condition sets the *minimum step-number*:

$$L_{\text{sim}} > \mathcal{H}\tau \tag{III.26}$$

The minimum step-number is used to *lower-bound* the computational cost of TI-PFA (Equation III.21):

$$\mathcal{T}_c\left\{\text{TI-PFA}\right\} \geq \left\{\; \Lambda\; \text{Max}\big(\mathcal{H}\tau, 1\big) - 1 \;\right\} t_{\text{op}}\; d^3 \tag{III.27}$$

$$\geq \left\{\; \text{Max}\big(\mathcal{H}\tau, 1\big) - 1 \;\right\} t_{\text{op}}\; d^3 \tag{III.28}$$

IV. STROBOSCOPIC EXPONENTIATION ALGORITHM

The *stroboscopic exponentiation algorithm* (SEA) leverages Hamiltonian periodicity for time-efficient quantum-simulation.

A. Stroboscopic Simulation

1. Periodic Hamiltonians

A *periodic Hamiltonian* has *discrete time-translational symmetry* with period T:

$$\hat{H}_{p,\text{sim}}(t+T) = \hat{H}_{p,\text{sim}}(t) \tag{IV.1}$$

2. Stroboscopic Evolution Operator

The simulation time can be expressed as follows:[5]

$$\tau = k\,\lambda\,T + \Delta t, \qquad k \in \mathbb{N}\,,\, \lambda \in \mathbb{N}_1 \tag{IV.2}$$

The *periodic evolution operator* obeys the following [238]:

$$\hat{U}_{p,\text{sim}}(\tau) = \left\{\hat{U}_{p,\text{sim}}(\Delta t)\right\}\left\{\hat{U}_{p,\text{sim}}\big(\lambda T\big)\right\}^k \tag{IV.3}$$

3. Stroboscopic Simulation Algorithm

The *stroboscopic simulation algorithm* (SSA) [239] can be represented schematically in two stages (Figure 8):

I. Aliasing: Obtain the base time-symmetry evolution operator and the remainder evolution operator.

II. Matrix Multiplication: Generate the periodic evolution operator using ordered products.

[5] $\mathbb{N} : \{0, 1, 2, \cdots, \infty\}$ $\quad$ $\mathbb{N}_1 : \{1, 2, \cdots, \infty\}$

a. Aliasing

The *base time-symmetry evolution operator* is the following:

$$\hat{U}_{\text{sym}}^{(0)} = \left[\mathcal{T} \left\{ e^{-i \int_0^T dt' \; \hat{H}_{p,\text{sim}}(t')} \right\} \right]^{\lambda} \tag{IV.4}$$

The *remainder evolution operator* is the following:

$$\hat{U}_{\text{rem}} = \mathcal{T} \left\{ e^{-i \int_0^{\Delta t} dt' \; \hat{H}_{p,\text{sim}}(t')} \right\} \tag{IV.5}$$

b. Matrix Multiplication

The *time-symmetry evolution operator* is the following:

$$\hat{U}_{\text{sym}} = \left\{ \hat{U}_{\text{sym}}^{(0)} \right\}^{k} \tag{IV.6}$$

The periodic evolution operator is the following:

$$\hat{U}_{p,\text{sim}}(\tau) = \left\{ \hat{U}_{\text{rem}} \right\} \left\{ \hat{U}_{\text{sym}} \right\} \tag{IV.7}$$

4. Computational Cost

a. Aliasing Cost

The base time-symmetry evolution operator and the remainder evolution operator are both approximated with TI-PFA (Equation III.28):

$$\mathcal{T}_c \left\{ \hat{U}_{a,\text{sym}}^{(0)} \right\} \geq \left\{ \text{Max}\Big(\mathcal{H}\, T, 1 \Big) + \lambda - 2 \right\} t_{\text{op}} \; d^3 \tag{IV.8}$$

$$\mathcal{T}_c \left\{ \hat{U}_{a,\text{rem}} \right\} \geq \left\{ \text{Max}\Big(\mathcal{H}\, \Delta t, 1 \Big) - 1 \right\} t_{\text{op}} \; d^3 \tag{IV.9}$$

b. Matrix Multiplication Cost

The computational cost of generating the ordered product is the following:

$$\mathcal{T}_c \Big\{ \text{Multiplication} \Big\} = k \; t_{\text{op}} \; d^3 \tag{IV.10}$$

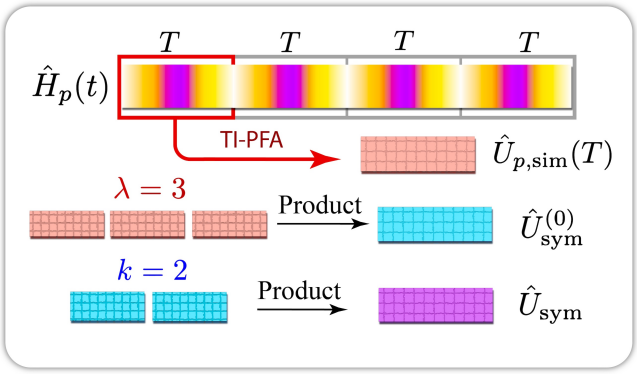

FIG. 8: The periodic evolution operator is generated for one period (red). The base time-symmetry evolution operator (blue) and the time-symmetry evolution operator (purple) are generated using matrix multiplication.

c. Minimum Algorithm Cost

The computational cost of SSA is lower-bounded by the following:

$$\mathcal{T}_c \Big\{ \text{SSA} \Big\} \geq \Bigg\{ \text{Max}\Big(\mathcal{H}\left(T + \Delta t\right), 2 \Big) + \Big(\lambda - 3 \Big) + k \Bigg\} t_{\text{op}} \; d^3 \tag{IV.11}$$

d. Parametrized Minimum Algorithm Cost

The computational cost of SSA can be parametrized as follows (Equation IV.2):

$$\mathcal{T}_c \Big\{ \text{SSA} \Big\} \geq \Bigg\{ \text{Max}\Big(\mathcal{H}\left(T + \Delta t\right), 2 \Big) + \Big(\lambda - 3 \Big) + \frac{\tau - \Delta t}{\lambda T} \Bigg\} t_{\text{op}} \; d^3 \tag{IV.12}$$

5. Quantum–Simulation Error

The error in SSA is the following (Equation III.23):

$$\epsilon_{\text{SSA}} \sim \left(k\, \lambda \right) \epsilon_{\text{TI-PFA}} \tag{IV.13}$$

$$\epsilon_{\text{SSA}} \sim \left(k\, \lambda \right) \mathcal{H} T \; \mathcal{O}\big(E_{\text{sub}} \big) \tag{IV.14}$$

$$\epsilon_{\text{SSA}} \sim \mathcal{H} \tau \; \mathcal{O}\big(E_{\text{sub}} \big) \tag{IV.15}$$

B. Stroboscopic Exponentiation Algorithm

1. Stroboscopic Evolution Operator

The simulation time can be expressed as follows:

$$\tau = k\,\lambda\,T + \Delta t, \qquad k \in \mathbb{N}\,,\,\lambda \in \mathbb{N}_1 \tag{IV.16}$$

The integer k is expressed using *binary notation* [240]:

$$k = \sum_{n=0}^{\mathcal{K}} k_n\,2^n, \qquad k_n \in \{0,1\} \tag{IV.17}$$

The periodic evolution operator obeys the following:

$$\hat{U}_{p,\mathrm{sim}}(\tau) = \left\{\hat{U}_{p,\mathrm{sim}}(\Delta t)\right\}\left[\prod_{\substack{n=0\\ \leftarrow}}^{\mathcal{K}}\left\{\hat{U}_{p,\mathrm{sim}}\left(2^n\,\lambda\,T\right)\right\}^{k_n}\right] \tag{IV.18}$$

2. Stroboscopic Exponentiation Algorithm

SEA can be represented schematically in three stages (Figure 9):

I. Aliasing: Obtain the base time-symmetry evolution operator and the remainder evolution operator.

II. Exponentiation: Perform recursive multiplication on the base time-symmetry evolution operator.

III. Matrix Multiplication: Generate the periodic evolution operator using ordered products.

a. Aliasing

The base time-symmetry evolution operator and remainder evolution operator are defined in Section IV A 3 a.

b. Exponentiation

The *exponentiated time-symmetry evolution operators* are the following:

$$\hat{U}_{\mathrm{sym}}^{(n)} = \left(\hat{U}_{\mathrm{sym}}^{(0)}\right)^{2^n} \tag{IV.19}$$

The exponentiated time-symmetry evolution operators are generated recursively:

$$\hat{U}_{\mathrm{sym}}^{(n)} = \left(\hat{U}_{\mathrm{sym}}^{(n-1)}\right)^{2} \tag{IV.20}$$

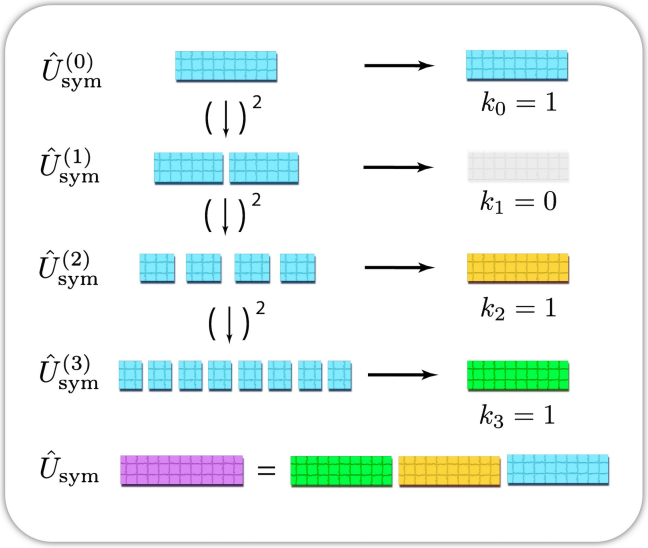

FIG. 9: The exponentiated time-symmetry evolution operators are generated recursively (left). The binary decomposition (right) is used to generate the time-symmetry evolution operator (bottom).

c. Matrix Multiplication

The time-symmetry evolution operator is as follows:

$$\hat{U}_{\mathrm{sym}} = \prod_{\substack{n=0\\ \leftarrow}}^{\mathcal{K}}\left\{\hat{U}_{\mathrm{sym}}^{(n)}\right\}^{k_n} \tag{IV.21}$$

The periodic evolution operator is the following:

$$\hat{U}_{p,\mathrm{sim}}(\tau) = \left\{\hat{U}_{\mathrm{rem}}\right\}\left\{\hat{U}_{\mathrm{sym}}\right\} \tag{IV.22}$$

3. Computational Cost

a. Aliasing Cost

The base time-symmetry evolution operator and the remainder evolution operator are generated as in Section IV A 4 a.

b. Exponentiation Cost

The computational cost of generating the exponentiated time-symmetry operators is the following:

$$\mathcal{T}_c\left\{\hat{U}_{\mathrm{sym}}^{(n)}\right\} = \mathcal{K}\;t_{\mathrm{op}}\;d^3 \tag{IV.23}$$

c. Matrix Multiplication Cost

The computational cost of generating the ordered product is the following:

$$\mathcal{T}_c\Big\{\text{Multiplication}\Big\} = \Big(\sum_{n=0}^{\mathcal{K}} k_n\Big)\, t_{\text{op}}\, d^3 \tag{IV.24}$$

d. Minimum Algorithm Cost

The computational cost of SEA is lower-bounded by the following:

$$\mathcal{T}_c\Big\{\text{SEA}\Big\} \geq \Bigg\{ \text{Max}\Big(\mathcal{H}\big(T+\Delta t\big), 2\Big) + \Big(\lambda + \mathcal{K} - 3\Big) + \sum_{n=0}^{\mathcal{K}} k_n \Bigg\}\, t_{\text{op}}\, d^3 \tag{IV.25}$$

e. Binary Constraint

The binary decomposition constrains the number of exponentiated time-symmetry operators:

$$\lambda\, T\, 2^{(\mathcal{K}+1)} > \tau - \Delta t \tag{IV.26}$$

$$\mathcal{K} > \log_2\left(\frac{\tau - \Delta t}{2\lambda T}\right) \tag{IV.27}$$

f. Parametrized Minimum Algorithm Cost

The computational cost of SEA can be parametrized as follows:

$$\mathcal{T}_c\Big\{\text{SEA}\Big\} \geq \Bigg\{ \text{Max}\Big(\mathcal{H}\big(T+\Delta t\big), 2\Big) + \Big(\lambda - 3\Big) + \text{Max}\left(\log_2\left(\frac{\tau - \Delta t}{2\lambda T}\right), 0\right) \Bigg\}\, t_{\text{op}}\, d^3 \tag{IV.28}$$

4. Quantum–Simulation Error

The error in SEA is the following (Equation IV.13):

$$\epsilon_{\text{SEA}} = \mathcal{H}\tau\ \ \mathcal{O}\big(E_{\text{sub}}\big) \tag{IV.29}$$

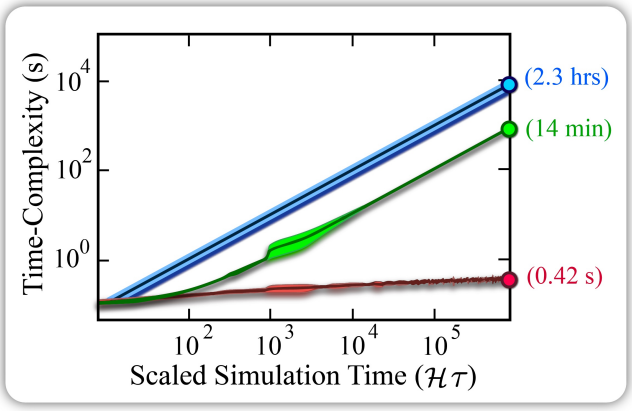

FIG. 10: The computational cost required to apply TI-PFA (blue), SSA (green), and SEA (red) to a 10-qubit periodic Hamiltonian is empirically determined.

C. Algorithm Comparison

1. Asymptotic Cost Analysis

The *asymptotic computational costs* of the quantum-simulation algorithms are the following:

$$\lim_{\tau\to\infty} \mathcal{T}_c\Big\{\text{TI-PFA}\Big\} \gtrsim \mathcal{H}\tau\ t_{\text{op}}\, d^3 \tag{IV.30}$$

$$\lim_{\tau\to\infty} \mathcal{T}_c\Big\{\text{SSA}\Big\} \gtrsim \frac{\tau}{\lambda T}\ t_{\text{op}}\, d^3 \tag{IV.31}$$

$$\lim_{\tau\to\infty} \mathcal{T}_c\Big\{\text{SEA}\Big\} \gtrsim \log_2\left(\frac{\tau}{\lambda T}\right)\ t_{\text{op}}\, d^3 \tag{IV.32}$$

a. Relative Algorithm Performance

SEA achieves an exponential speed-up over TI-PFA and SSA in simulating periodic Hamiltonians (Figure 10).

V. TRAP SIM II

Trap Sim II is a proprietary MATLAB code that performs time-efficient quantum-simulation of ion trap quantum computers.

A. Hamiltonian Periodicity

1. Schrödinger Picture Hamiltonian

The *laser period* is the following:

$$T_{\text{laser}} = \frac{2\pi}{\omega} \tag{V.1}$$

The *Schrödinger picture Hamiltonian* is periodic:

$$\hat{H}_{\text{ion trap}}\left(t + T_{\text{laser}}\right) = \hat{H}_{\text{ion trap}}(t) \tag{V.2}$$

2. Interaction Picture Hamiltonian

The interaction picture Hamiltonian is not periodic in general (Equation II.73).

B. Regularization Effects

1. Hamiltonian Regularization

A *bosonic truncation* is placed on the ladder operators [241–248]:

$$\hat{a}_{\zeta}^{\dagger}\,|n\rangle = 0, \quad \forall\, n \geq \zeta \tag{V.3}$$

The *regularized effective ion trap Hamiltonian* is the following (Equation II.68):

$$\hat{H}^{(\zeta)}_{\text{eff, ion trap}}(t) = \sum_{k=1}^{3N} \tilde{\omega}_k \left\{ \hat{a}^{\dagger}_{k,\zeta}\, \hat{a}_{k,\zeta} \right\} + \hat{H}_{\text{qubit}}(t) \tag{V.4}$$

2. Computer Memory

The dimension of the Hilbert space is the following:

$$\dim\left\{ \mathcal{H}_{\text{ion trap}} \right\} = 2^N \left(\zeta + 1\right)^{3N} \tag{V.5}$$

The memory required to perform quantum-simulation on a 64-bit processor is the following (Figure 11):

$$\text{Memory}\left\{ \mathcal{H}_{\text{ion trap}} \right\} = 16\,\text{bytes} \times 4^N \left(\zeta + 1\right)^{6N} \tag{V.6}$$

3. Bosonic Saturation

The *vibrational occupation operators* are as follows [249]:

$$\hat{\mathcal{N}}_k = \hat{a}_k^{\dagger}\, \hat{a}_k \tag{V.7}$$

The *vibrational occupation uncertainties* are as follows:

$$\sigma_{\mathcal{N}_k} = \sqrt{\left\langle \hat{\mathcal{N}}_k^2 \right\rangle - \left\langle \hat{\mathcal{N}}_k \right\rangle^2} \tag{V.8}$$

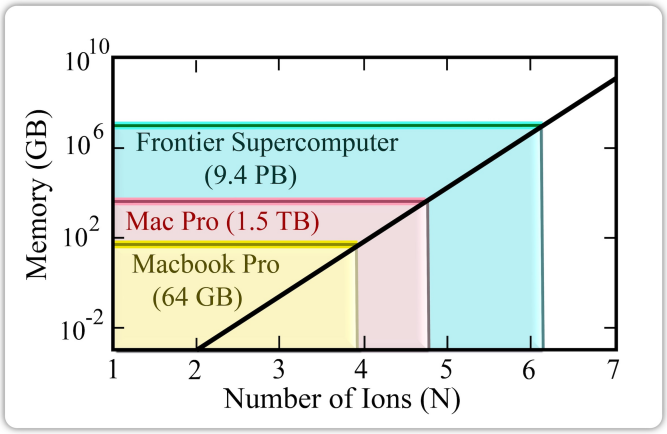

FIG. 11: The *threshold simulation memory* (black) is compared with the *random access memory* of several classical computing platforms (colored) [250–252].

If the bosonic truncation is saturated, an accumulation of *regularization effects* ensure that the simulation can no longer be compared to nature:

$$\text{Bosonic Saturation:} \quad \left\langle \hat{\mathcal{N}}_k \right\rangle \pm \sigma_{\mathcal{N}_k} \sim \zeta \tag{V.9}$$

C. Anisotropic Randomized Truncation

Anisotropic Randomized Truncation (ART) is used to estimate the size of regularization effects. It can be represented schematically in three stages:

I. Truncation: Regularize the Hamiltonian randomly.

II. Quantum-Simulation: Generate an evolution operator for the regularized Hamiltonians.

III. Error-Estimation: Estimate the regularization effects using quantum channel technology.

1. Truncation

The vibrational modes are regularized anisotropically (Figure 12):

$$\hat{H}^{(\vec{\zeta})}_{\text{eff, ion trap}}(t) = \sum_{k=1}^{3N} \tilde{\omega}_k \left\{ \hat{a}^{\dagger}_{k,\zeta_k}\, \hat{a}_{k,\zeta_k} \right\} + \hat{H}_{\text{qubit}}(t) \tag{V.10}$$

Regularized Hamiltonians are selected pseudo-randomly to generate the *ART Hamiltonian set*:

$$\mathcal{A}_{\mathcal{H}} = \left\{ \hat{H}^{(\vec{\zeta}_1)}_{\text{eff, ion trap}}(t)\,,\ \cdots\ ,\ \hat{H}^{(\vec{\zeta}_{Na})}_{\text{eff, ion trap}}(t) \right\} \tag{V.11}$$

2. Quantum–Simulation

a. Regularized Evolution Operators

The *regularized evolution operators* are the following:

$$\hat{U}_{\text{reg}}(\vec{\zeta}) = \mathcal{T}\left\{ e^{-i\int_0^{\mathcal{T}} dt' \; \hat{H}^{(\vec{\zeta})}_{\text{eff, ion trap}}(t')} \right\} \tag{V.12}$$

b. Haar Measure

The *regularized Haar measure* is a subset of the *Haar measure* [253–256] composed of the regularized evolution operators (Figure 13):

$$\mathcal{U}_{\text{reg}} = \left\{ \hat{U}_{\text{reg}}(\vec{\zeta}), \; \forall \; \vec{\zeta} \right\} \tag{V.13}$$

$$\mathcal{U}_{\text{reg}} \subseteq \mathcal{U}_{\text{Haar}} \tag{V.14}$$

The *ART unitary set* is the following:

$$\mathcal{A}_{\mathcal{U}} = \left\{ \hat{U}_{\text{reg}}(\vec{\zeta}_1) \; , \cdots , \; \hat{U}_{\text{reg}}(\vec{\zeta}_{Na}) \right\} \tag{V.15}$$

$$\mathcal{A}_{\mathcal{U}} \subseteq \mathcal{U}_{\text{reg}} \tag{V.16}$$

3. Error–Estimation

Simulated Expectation-Value Approximate Reconstruction (SEAR) is used to approximate the regularization effects [257].

a. Quantum Channel Technology

A *superoperator* on a Hilbert space $\mathcal{H}$ has the following form [258]:

$$\tilde{\mathcal{E}} = \sum_{\mu=1}^{\mathcal{R}} \hat{K}_\mu \otimes \hat{K}_\mu^\dagger \tag{V.17}$$

$$\hat{K}_\mu \in \mathcal{H} \otimes \mathcal{H}^* \tag{V.18}$$

A *quantum channel* is a type of superoperator. Its *Kraus operators* [259] satisfy the following condition [260]:

$$\sum_{\mu=1}^{\mathcal{R}} \hat{K}_\mu \hat{K}_\mu^\dagger = \hat{\mathbb{1}} \tag{V.19}$$

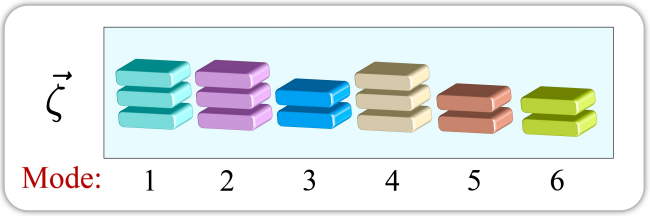

FIG. 12: The maximum number of vibrational excitations (colored) is set independently for each mode.

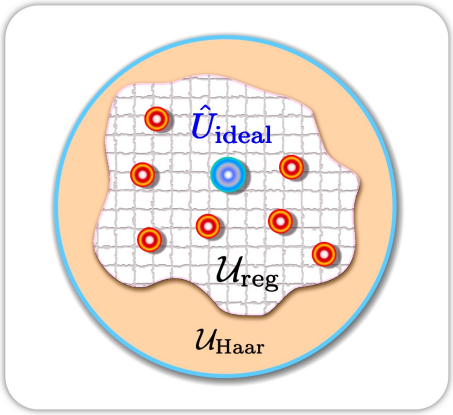

FIG. 13: ART generates unitary operators (red) from the regularized Haar measure (gray), which contains the ideal evolution operator (blue).

The action of a quantum channel on a state $|\psi\rangle$ generates a *density matrix* [260–262]:

$$\tilde{\mathcal{E}}\left(|\psi\rangle \right) = \sum_{\mu=1}^{\mathcal{R}} \hat{K}_\mu \left(\; |\psi\rangle\langle\psi| \; \right) \hat{K}_\mu^\dagger \tag{V.20}$$

b. Quantum Channel Averaging

Applying a *similarity transformation* to a quantum channel yields the following [263]:

$$\tilde{\mathcal{E}}_{\mathbf{u}} = \tilde{\mathcal{U}}^\dagger \; \tilde{\mathcal{E}} \; \tilde{\mathcal{U}} \tag{V.21}$$

$$= \sum_{\mu=1}^{\mathcal{R}} \hat{U}^\dagger \hat{K}_\mu \hat{U} \; \otimes \; \hat{U}^\dagger \hat{K}_\mu^\dagger \hat{U} \tag{V.22}$$

Averaging a quantum channel over the Haar measure yields a *depolarizing channel* (Figure 14) [263, 264]:

$$\tilde{\mathcal{D}}_\epsilon = \int d\mathcal{U}_{\text{Haar}} \; \tilde{\mathcal{U}}^\dagger \; \tilde{\mathcal{E}} \; \tilde{\mathcal{U}} \tag{V.23}$$

$$\tilde{\mathcal{D}}_\epsilon\left(\rho \right) = (1-\epsilon)\,\rho + \epsilon \, \frac{\mathbb{1}}{\dim(\mathcal{H})} \tag{V.24}$$

The depolarizing channel has a characteristic *noise strength* [265–292]:

$$\epsilon = 1 - \frac{\mathrm{Tr}\left(\tilde{\mathcal{E}}\right) - 1}{\left[\dim\left(\mathcal{H}\right)\right]^2 - 1} \tag{V.25}$$

$$0 \leq \epsilon \leq 1 \tag{V.26}$$

c. Approximate Quantum Simulation

The *ideal evolution operator* has an arbitrarily large bosonic truncation (Figure 13):

$$\hat{U}_{\text{ideal}} = \hat{U}_{\text{reg}}(\infty) \tag{V.27}$$

The *ideal output state* is the following:

$$\rho_{\text{ideal}} = \hat{U}_{\text{ideal}} \left(\ |\psi\rangle\langle\psi| \ \right) \hat{U}_{\text{ideal}}^{\dagger} \tag{V.28}$$

The *regularized output states* are the following:

$$\rho_{\text{reg}}^{(\vec{\zeta})} = \hat{U}_{\text{reg}}(\vec{\zeta}) \left(\ |\psi\rangle\langle\psi| \ \right) \hat{U}_{\text{reg}}^{\dagger}(\vec{\zeta}) \tag{V.29}$$

Averaging the regularized output states generated by the ART unitary set yields the *ART output state*:

$$\rho_{\text{ART}} = \frac{1}{N_a} \sum_{\mu=1}^{N_a} \rho_{\text{reg}}^{(\vec{\zeta}_\mu)} \tag{V.30}$$

d. SEAR Error Channel

The *SEAR error channel* maps the ideal output state to the ART output state:

$$\tilde{\mathcal{S}}\left(\rho_{\text{ideal}}\right) = \rho_{\text{ART}} \tag{V.31}$$

The *SEAR error channel* is written explicitly:

$$\tilde{\mathcal{S}} = \frac{1}{N_a} \sum_{\mu=1}^{N_a} \hat{U}_{\text{SEAR}}(\vec{\zeta}_\mu) \ \otimes \ \hat{U}_{\text{SEAR}}^{\dagger}(\vec{\zeta}_\mu) \tag{V.32}$$

$$\hat{U}_{\text{SEAR}}\left(\vec{\zeta}_\mu\right) = \hat{U}_{\text{reg}}(\vec{\zeta}_\mu) \, \hat{U}_{\text{ideal}}^{\dagger} \tag{V.33}$$

The *SEAR noise strength* is the following:

$$\epsilon_{\text{SEAR}} = 1 - \frac{\mathrm{Tr}\left(\tilde{\mathcal{S}}\right) - 1}{\left[\dim\left(\mathcal{H}\right)\right]^2 - 1} \tag{V.34}$$

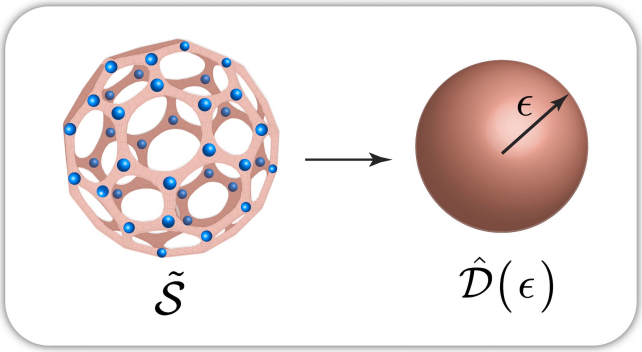

FIG. 14: The SEAR error channel (left) is defined using its *kraus operators* (blue). Averaging the SEAR error channel generates a depolarizing channel (right).

e. Regularization Effects

The SEAR error channel forces observables to stray from their ideal values, causing *truncation fluctuations*:

$$\Delta O_{\text{trunc}} = \left| \ \left\langle \psi \left| \hat{U}_{\text{ideal}}^{\dagger} \, \hat{O} \, \hat{U}_{\text{ideal}} \right| \psi \right\rangle - \mathrm{Tr}\left\{ \ \tilde{\mathcal{S}}\left(\rho_{\text{ideal}}\right) \hat{O} \ \right\} \ \right| \tag{V.35}$$

The *average truncation fluctuation* can be bounded using the SEAR noise strength [257]:

$$\overline{\Delta O}_{\text{trunc}} \ \leq \ \epsilon_{\text{SEAR}} \left| O_{\text{eigenvalue}}^{max} - O_{\text{eigenvalue}}^{min} \right| \tag{V.36}$$

f. Noise Spectroscopy

The *complementary SEAR error channels* are generated by substituting the ideal evolution operator with the regularized evolution operators (Equation V.33):[6]

$$\tilde{\mathcal{S}}_\eta = \frac{1}{N_a} \sum_{\mu=1}^{N_a} \hat{U}_{\text{SEAR}}^{(\eta)}(\vec{\zeta}_\mu) \ \otimes \ \hat{U}_{\text{SEAR}}^{(\eta)\,\dagger}(\vec{\zeta}_\mu) \tag{V.37}$$

$$\hat{U}_{\text{SEAR}}^{(\eta)}\left(\vec{\zeta}_\mu\right) = \hat{U}_{\text{reg}}(\vec{\zeta}_\mu) \, \hat{U}_{\text{reg}}^{\dagger}(\vec{\zeta}_\eta) \tag{V.38}$$

The *complementary SEAR noise strength* can be estimated using *measurement protocols* [257, 264].

D. Numerical Results

Trap Sim II is used to simulate an ion trap quantum computer.

[6] The SEAR error channel cannot be studied directly due to the inaccessibility of the ideal evolution operator.

1. Simulation Goals

The simulation is performed to examine the following:

I. Bosonic Saturation

II. Regularization Effects

III. Entanglement Growth

IV. Weak-Laser Approximation (WLA)

2. Simulation Parameters

The simulation parameters are the following [156, 157]:

$$\text{Number of Ions}: \ N = 1 \tag{V.39}$$

$$\text{Ion Charge}: \ Q = +e \tag{V.40}$$

$$\text{Ion Mass}: \ M \sim 200 \text{ GeV} \tag{V.41}$$

$$\text{Physical Trap Frequency}: \ \tilde{\omega}_a \sim 1 \text{ MHz} \tag{V.42}$$

$$\text{Laser Wavelength}: \ \lambda \sim 400 \text{ nm} \tag{V.43}$$

$$\text{Laser Power}: \ P_{\text{laser}} \sim 1 \text{ W} \tag{V.44}$$

$$\text{Bosonic Truncation}: \ \zeta \sim 6 \tag{V.45}$$

$$\text{Trap Potential}: \text{XY-Symmetric \& Harmonic} \tag{V.46}$$

3. Numerical Results

a. Bosonic Saturation

The vibrational occupation is computed throughout the simulation (Figure 15, Figure 16).

Computational Details:

- The ion trap is initialized in the motional ground-state [293–321].

b. Regularization Effects

The SEAR noise strength is approximated using ART (Figure 17, Figure 18).

Computational Details:

- Eight anisotropic bosonic truncations are chosen.
- The SEAR noise strength is estimated repeatedly.
- A bootstrap algorithm [322, 323] is used to generate an uncertainty in the average SEAR noise strength estimate.

c. Entanglement Growth

The *von Neumann entanglement entropy* [324] of the qubit is computed throughout the simulation (Figure 19, Figure 20):[7]

$$\mathcal{S}(\rho) = -\text{Tr}\Big(\rho \log(\rho)\Big) \tag{V.47}$$

Computational Details:

- The qubit is initialized in 10^2 pseudo-randomly generated *pure states* [390].
- A bootstrap algorithm is used to generate an uncertainty in the average entanglement entropy.

d. Effective Hamiltonian Validity

The WLA error is computed (Figure 21, Figure 22).

Computational Details:

- The qubit is initialized in 10^2 pseudo-randomly generated pure states.
- The Pauli operator $\hat{\sigma}_z$ is measured.
- A bootstrap algorithm is used to generate an uncertainty in the average WLA error.

4. Empirical Observations

a. Bosonic Saturation

After the onset of bosonic saturation, the vibrational occupation exhibits unphysical behavior (Figure 16).

Commentary:

- Bosonic saturation places a temporal limit on the amount of ion trap dynamics that can be probed numerically.
- This suggests that ion trap quantum-simulation be used as a *performance heuristic* for quantum-simulation protocols [391].
- The (N, ζ, ϵ) ion-trap performance heuristic is the following:

> *A quantum-simulation protocol passes the (N, ζ, ϵ) ion-trap performance heuristic by performing quantum-simulation of the N-ion, ζ-cutoff ion trap Hamiltonian until bosonic saturation is observed, with total error bounded by ϵ.*

[7] The entanglement entropy is a wildly important quantity, with applications to many areas of physics [325–389].

b. *Regularization Effects*

The noise strength increases with simulation time, and experiences a sharp growth during the onset of bosonic saturation (Figure 18).

Commentary:

- Each ART Hamiltonian generates a different set of regularization effects due to the anisotropic bosonic truncation.
- The SEAR noise strength provides a measure of the disparity between the ART unitary operators (Equation V.33).
- The ART unitary operators diverge during bosonic saturation, and the average error grows to $\gtrsim 60\%$.

c. *Entanglement Growth*

The entanglement entropy of the qubit increases with simulation time until the onset of bosonic saturation. The entanglement entropy then fluctuates non-trivially (Figure 20).

Commentary:

- The entanglement entropy is expected to increase as the purity of the qubit is lost to the environment [392–398].
- Bosonic saturation restricts the *decoherence times* [399] that can be probed numerically:
  - *Decoherence cannot be observed numerically unless the qubits are sufficiently noisy.*

d. *Effective Hamiltonian Validity*

WLA accumulates $\sim 1\%$ error after the onset of bosonic saturation (Figure 22).

Commentary:

- The stability of approximations such as the *rotating-wave approximation* [400–410], the *Lamb-Dicke limit* [411–416], and the *Magnus Expansion* [417–433] may be uncertain in the parameter regimes required for the most ambitious ion trap quantum computing proposals [434–443].[8]
- To conserve the limited and transient resources available to the scientific community at large, it is necessary to verify that perturbative protocols will succeed when implemented on real ion trap quantum computers, which are inherently non-perturbative.[9]
- Trap Sim II is a rigorous algorithm test-bed for up to six ions (Figure 11). The sole approximation made by Trap Sim II is that of finite bosonic truncation.

[8] Much of the pressing uncertainty is rooted in the intractability of the Magnus Expansion [444].

[9] For a successful instance of this paradigm, see [445, 446].

VI. APPENDIX

A. TI-PFA vs. Sampling PFA

The *sampling product-formula algorithm* (S-PFA) [166, 447] can be expressed schematically in two stages:

I. Sampling: Sample the Hamiltonian at set times and approximate the sub-region evolution operators.

II. Matrix Multiplication: Take the ordered product of the approximate sub-region evolution operators.

a. *Sampling*

The sub-region Hamiltonians are as follows (Equation III.9):

$$\hat{H}^{(r)}_{\text{sub}} = \hat{H}_{\text{sim}}\big((r-1)\,\delta t\big) \tag{VI.1}$$

The approximate sub-region evolution operators are the following:

$$\hat{U}^{(r)}_{a,\text{sub}} = e^{-i\,\delta t\,\hat{H}^{(r)}_{\text{sub}}} \tag{VI.2}$$

b. *Sub-Region Evolution Operator Error*

The *maximum eigenvalue derivative* of the Hamiltonian is the following:

$$\mathcal{D}_{\text{max}} = \left\{ \left| \frac{\partial}{\partial t}\,\mathcal{E}_\alpha(t) \right|_{\text{max}} \right\}_{\overline{\text{max}}\,\mathcal{T}} \tag{VI.3}$$

The error in the sub-region evolution operator is the following:

$$\hat{\mathcal{E}}^{(r)}_{\text{sub}} \sim \mathcal{D}_{\text{max}}\,\delta t + \mathcal{O}\left(E^2_{\text{sub}}\right) \tag{VI.4}$$

c. *Relative Algorithm Performance*

S-PFA struggles to resolve the true dynamics of the Hamiltonian due to sampling errors, which are not present in TI-PFA.

B. Regularization Effects

If the length-scale of the laser is sufficiently long, the severity of the regularization effects can be determined rigorously via an efficient classical computation [448].

ACKNOWLEDGEMENTS

Unjustly condemned, he was led away.

No one cared that he died without descendants,
that his life was cut short in midstream.

But he was struck down for
the rebellion of my people.

—Isaiah 53:8

— AMDG —

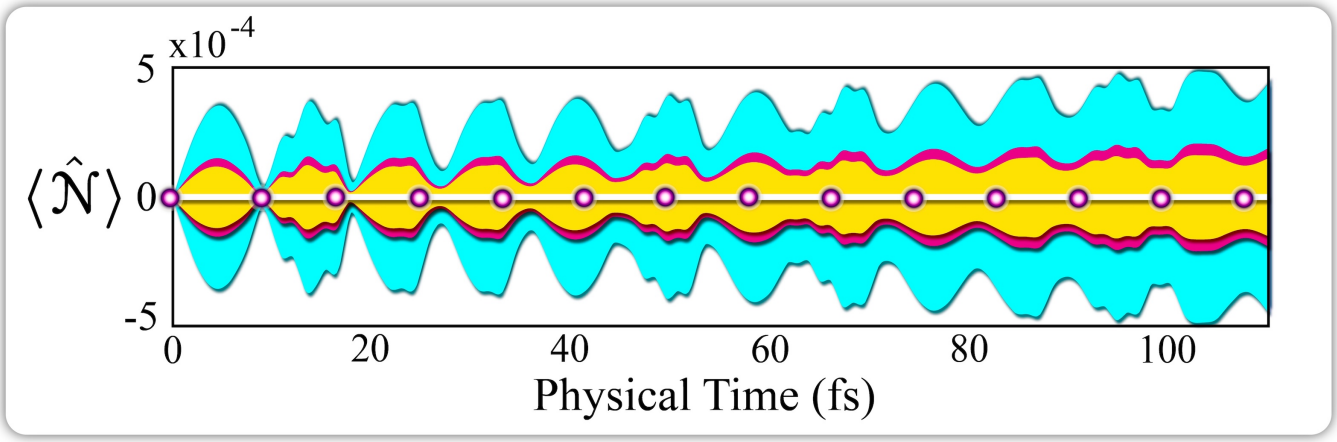

FIG. 15: On the laser timescale, the vibrational occupation of the X-mode (magenta), the Y-mode (yellow), and the Z-mode (cyan), fluctuates non-trivially around zero.[a]

[a] The uncertainty is amplified by a factor of 10^4. The observable is sampled 7.5 times faster than displayed.

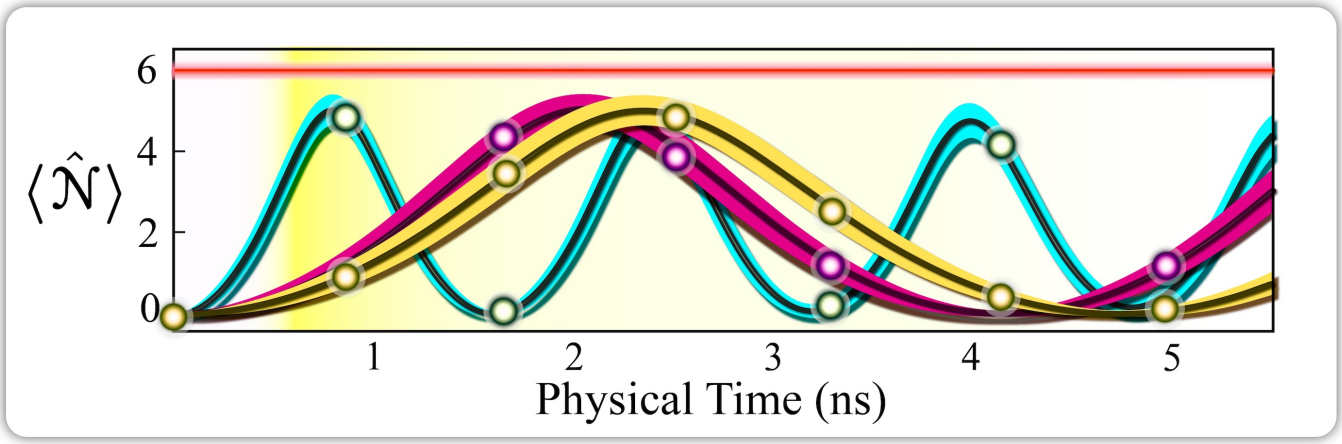

FIG. 16: The vibrational occupation of the modes grows until the bosonic truncation (red) is approached. The onset of bosonic saturation (yellow backdrop) results in unphysical oscillations of the vibrational occupation.[a]

[a] The uncertainty is suppressed by a factor of 3. The observable is sampled 7.5 times faster than displayed.

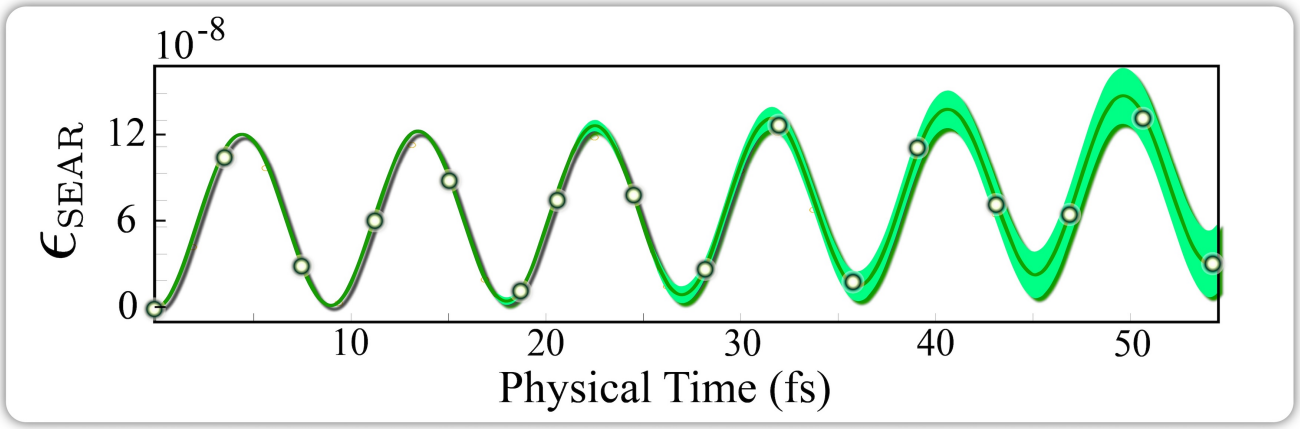

FIG. 17: On the laser timescale, the SEAR noise strength (green) is perturbatively small, indicating the initial accuracy of the quantum-simulation protocol.[a]

[a] The uncertainty is amplified by a factor of 8×10^4. The observable is sampled 3 times faster than displayed.

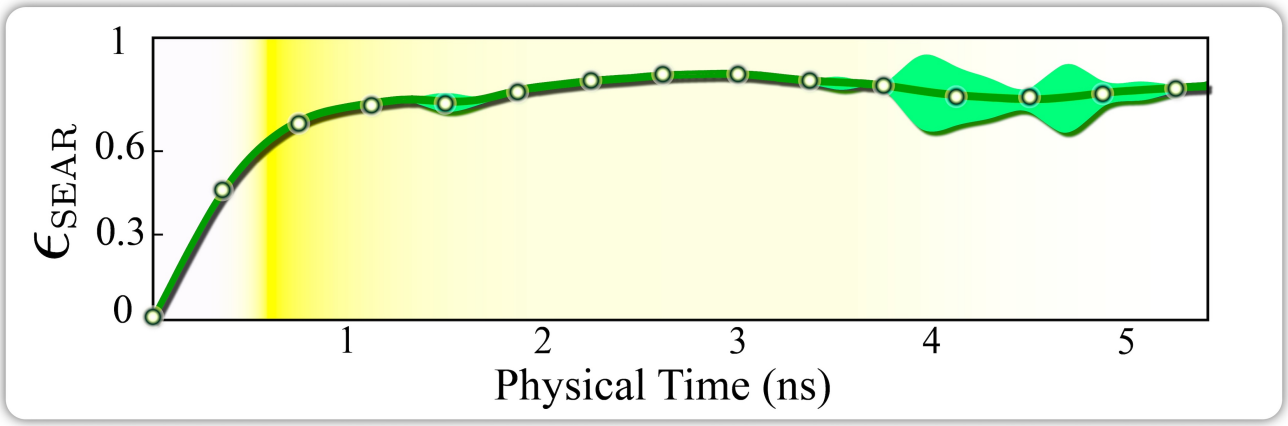

FIG. 18: The SEAR noise strength (green) approaches unity after the onset of bosonic saturation (yellow backdrop), indicating the ultimate failure of the quantum-simulation protocol.[a]

[a] The uncertainty is amplified by a factor of 5×10^2. The observable is sampled 3 times faster than displayed.

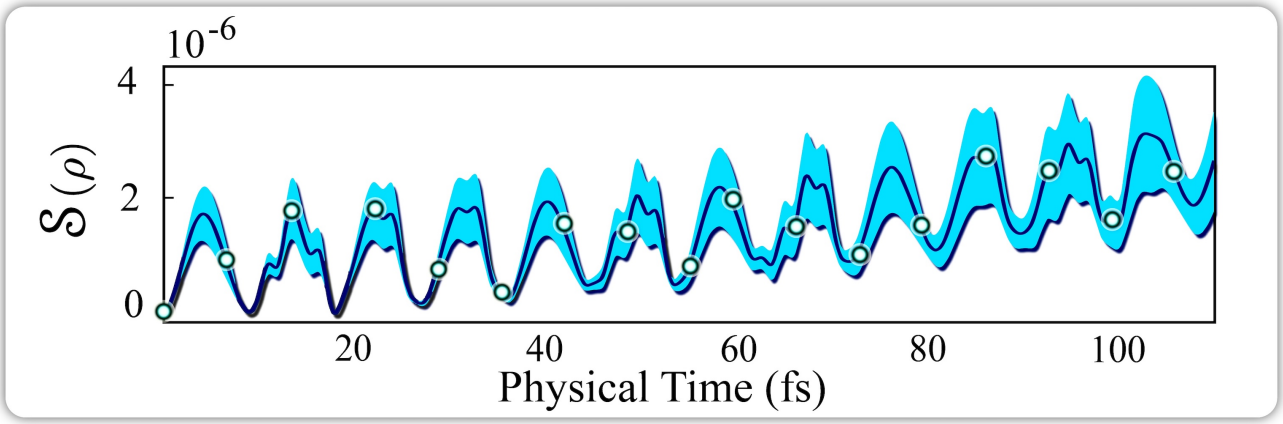

FIG. 19: On the laser timescale, the entanglement entropy (blue) fluctuates non-trivially as the qubit interacts with the vibrational modes.[a]

[a] The uncertainty is amplified by a factor of 2. The observable is sampled 6 times faster than displayed.

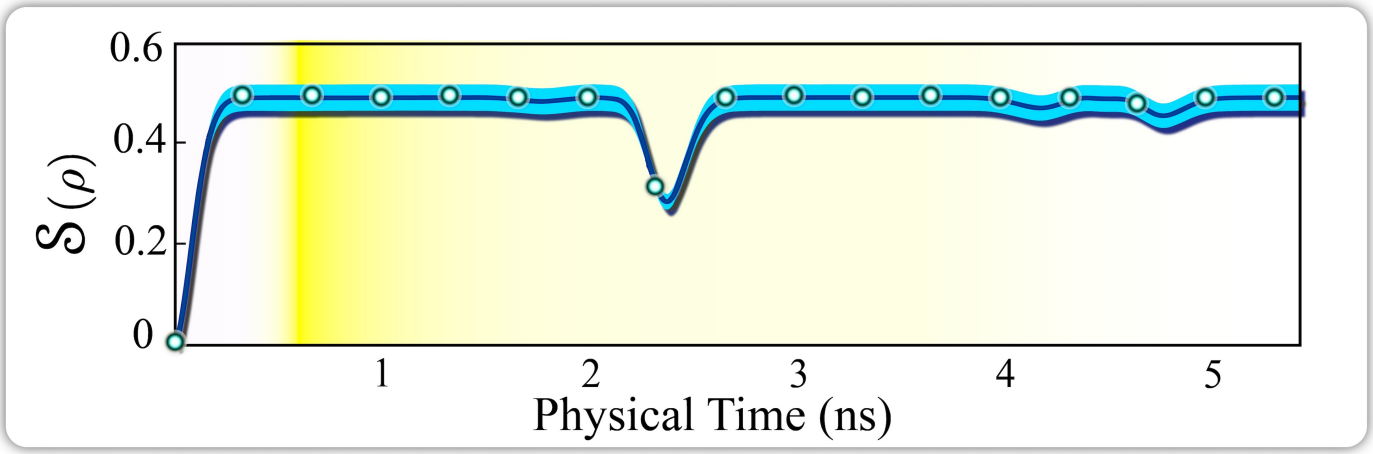

FIG. 20: The entanglement entropy (blue) ceases to grow after the onset of bosonic saturation (yellow backdrop), and the decoherence of the qubit is halted.[a]

[a] The observable is sampled 6 times faster than displayed.

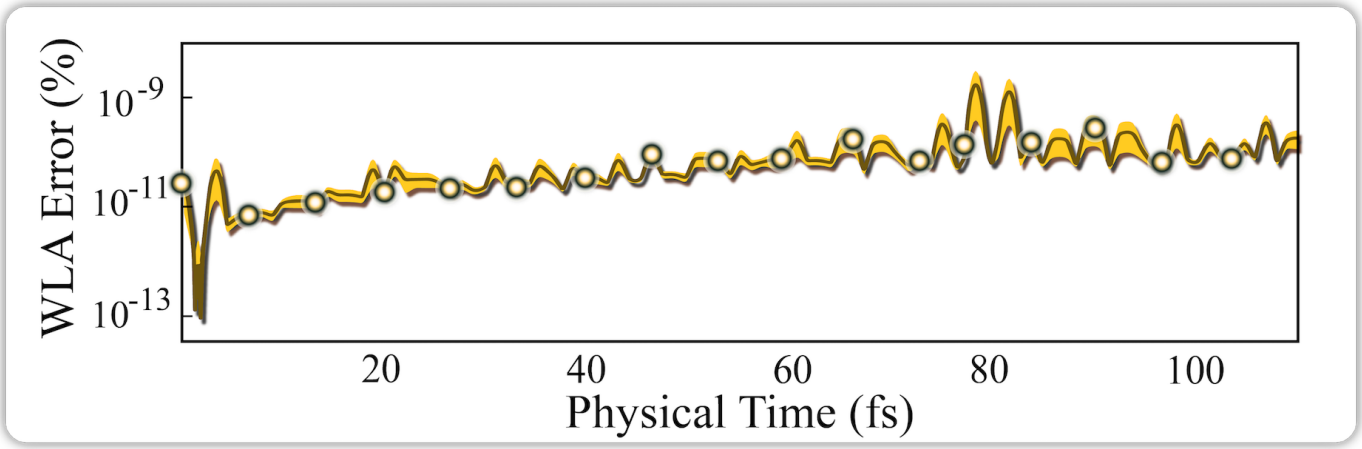

FIG. 21: Over the laser timescale, the WLA error (golden) increases by several orders of magnitude.[a]

[a] The observable is sampled 6 times faster than displayed.

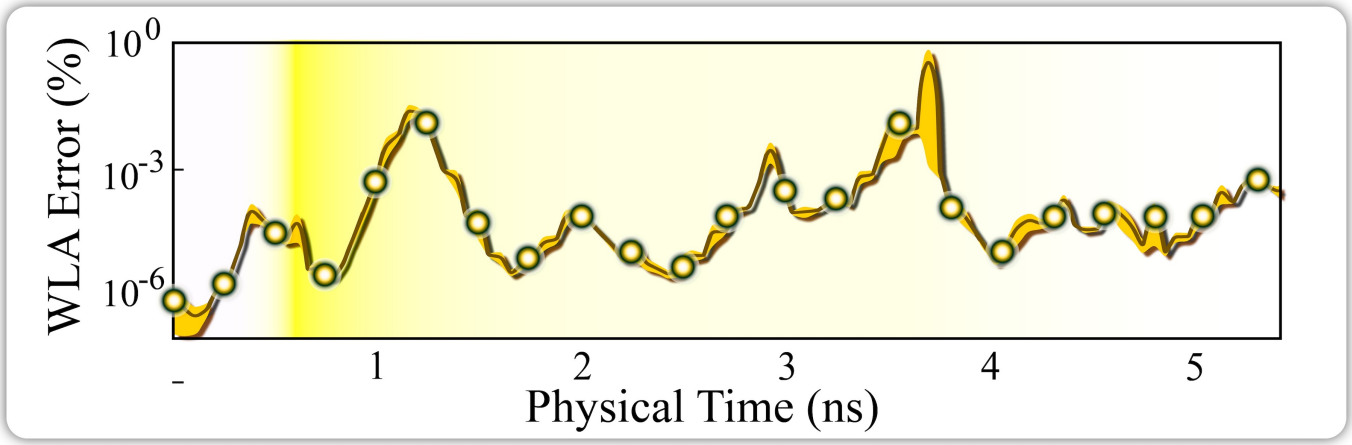

FIG. 22: The WLA error (golden) fluctuates non-trivially after the onset of bosonic saturation (yellow backdrop).[a]

[a] The observable is sampled 6 times faster than displayed.

[1] R. P. Feynman, Simulating physics with computers, International Journal of Theoretical Physics **21**, 467 (1982).

[2] J. I. Cirac and P. Zoller, Quantum computations with cold trapped ions, Phys. Rev. Lett. **74**, 4091 (1995).

[3] C. Monroe, D. M. Meekhof, B. E. King, W. M. Itano, and D. J. Wineland, Demonstration of a fundamental quantum logic gate, Phys. Rev. Lett. **75**, 4714 (1995).

[4] J. Koch, T. M. Yu, J. Gambetta, A. A. Houck, D. I. Schuster, J. Majer, A. Blais, M. H. Devoret, S. M. Girvin, and R. J. Schoelkopf, Charge-insensitive qubit design derived from the cooper pair box, Phys. Rev. A **76**, 042319 (2007).

[5] A. A. Houck, J. A. Schreier, B. R. Johnson, J. M. Chow, J. Koch, J. M. Gambetta, D. I. Schuster, L. Frunzio, M. H. Devoret, S. M. Girvin, and R. J. Schoelkopf, Controlling the spontaneous emission of a superconducting transmon qubit, Phys. Rev. Lett. **101**, 080502 (2008).

[6] S. Richer, N. Maleeva, S. T. Skacel, I. M. Pop, and D. DiVincenzo, Inductively shunted transmon qubit with tunable transverse and longitudinal coupling, Phys. Rev. B **96**, 174520 (2017).

[7] C.-P. Yang and Z.-F. Zheng, Deterministic generation of greenberger-horne-zeilinger entangled states of cat-state qubits in circuit qed, Opt. Lett. **43**, 5126 (2018).

[8] P. Winkel, I. Takmakov, D. Rieger, L. Planat, W. Hasch-Guichard, L. Grünhaupt, N. Maleeva, F. Foroughi, F. Henriques, K. Borisov, J. Ferrero, A. V. Ustinov, W. Wernsdorfer, N. Roch, and I. M. Pop, Nondegenerate parametric amplifiers based on dispersion-engineered josephson-junction arrays, Phys. Rev. Applied **13**, 024015 (2020).

[9] L.-N. Ji, T. Chen, and Z.-Y. Xue, Scalable nonadiabatic holonomic quantum computation on a superconducting qubit lattice, Phys. Rev. A **100**, 062312 (2019).

[10] J. Lisenfeld, A. Bilmes, A. Megrant, R. Barends, J. Kelly, P. Klimov, G. Weiss, J. M. Martinis, and A. V. Ustinov, Electric field spectroscopy of material defects in transmon qubits, npj Quantum Information **5**, 105 (2019).

[11] M. K. Ekström, T. Aref, A. Ask, G. Andersson, B. Suri, H. Sanada, G. Johansson, and P. Delsing, Towards phonon routing: Controlling propagating acoustic waves in the quantum regime, arXiv e-prints , arXiv:1909.07027 (2019), arXiv:1909.07027 [quant-ph].

[12] R. Yang and H. Deng, Fabrication of the impedance-matched josephson parametric amplifier and the study of the gain profile, IEEE Transactions on Applied Superconductivity **30**, 1 (2020).

[13] A. Kringhøj, T. W. Larsen, B. van Heck, D. Sabonis, O. Erlandsson, I. Petkovic, D. I. Pikulin, P. Krogstrup, K. D. Petersson, and C. M. Marcus, Controlled dc monitoring of a superconducting qubit, Phys. Rev. Lett. **124**, 056801 (2020).

[14] Y. Yanay, J. Braumüller, S. Gustavsson, W. D. Oliver, and C. Tahan, Two-dimensional hard-core bose–hubbard model with superconducting qubits, npj Quantum Information **6**, 58 (2020).

[15] D. Thanh Le, J. H. Cole, and T. M. Stace, Building a bigger hilbert space for superconducting devices, one bloch state at a time, Phys. Rev. Research **2**, 013245 (2020).

[16] D. Ristè, L. C. G. Govia, B. Donovan, S. D. Fallek, W. D. Kalfus, M. Brink, N. T. Bronn, and T. A. Ohki, Real-time processing of stabilizer measurements in a bit-flip code, npj Quantum Information **6**, 71 (2020).

[17] M. Kounalakis, Y. M. Blanter, and G. A. Steele, Flux-mediated optomechanics with a transmon qubit in the single-photon ultrastrong-coupling regime, Phys. Rev. Research **2**, 023335 (2020).

[18] A. Kringhøj, B. van Heck, T. W. Larsen, O. Erlandsson, D. Sabonis, P. Krogstrup, L. Casparis, K. D. Petersson, and C. M. Marcus, Suppressed charge dispersion via resonant tunneling in a single-channel transmon, Phys. Rev. Lett. **124**, 246803 (2020).

[19] A. Vepsäläinen, S. Danilin, and G. S. Paraoanu, Superadiabatic population transfer in a three-level superconducting circuit **5**, 10.1126/sciadv.aau5999 (2019).

[20] P. O. Guimond, B. Vermersch, M. L. Juan, A. Sharafiev, G. Kirchmair, and P. Zoller, A unidirectional on-chip photonic interface for superconducting circuits, npj Quantum Information **6**, 32 (2020).

[21] P. Winkel, K. Borisov, L. Grünhaupt, D. Rieger, M. Spiecker, F. Valenti, A. V. Ustinov, W. Wernsdorfer, and I. M. Pop, Implementation of a transmon qubit using superconducting granular aluminum, Phys. Rev. X **10**, 031032 (2020).

[22] I. Tsioutsios, K. Serniak, S. Diamond, V. V. Sivak, Z. Wang, S. Shankar, L. Frunzio, R. J. Schoelkopf, and M. H. Devoret, Free-standing silicon shadow masks for transmon qubit fabrication, AIP Advances **10**, 065120 (2020).

[23] A. Bargerbos, W. Uilhoorn, C.-K. Yang, P. Krogstrup, L. P. Kouwenhoven, G. de Lange, B. van Heck, and A. Kou, Observation of vanishing charge dispersion of a nearly open superconducting island, Phys. Rev. Lett. **124**, 246802 (2020).

[24] S. Hazra, K. V. Salunkhe, A. Bhattacharjee, G. Bothara, S. Kundu, T. Roy, M. P. Patankar, and R. Vijay, Engineering cross resonance interaction in multi-modal quantum circuits, Applied Physics Letters **116**, 152601 (2020).

[25] D. M. Abrams, N. Didier, B. R. Johnson, M. P. da Silva, and C. A. Ryan, Implementation of the XY interaction family with calibration of a single pulse, arXiv e-prints , arXiv:1912.04424 (2019), arXiv:1912.04424 [quant-ph].

[26] G. Andersson, M. K. Ekström, and P. Delsing, Electromagnetically induced acoustic transparency with a superconducting circuit, Phys. Rev. Lett. **124**, 240402 (2020).

[27] A. Bengtsson, P. Vikstål, C. Warren, M. Svensson, X. Gu, A. F. Kockum, P. Krantz, C. Križan, D. Shiri, I.-M. Svensson, G. Tancredi, G. Johansson, P. Delsing, G. Ferrini, and J. Bylander, Improved success probability with greater circuit depth for the quantum approximate optimization algorithm, Phys. Rev. Applied **14**, 034010 (2020).

[28] T. Liu, Q.-P. Su, Y. Zhang, Y.-L. Fang, and C.-P. Yang, Generation of quantum entangled states of multiple groups of qubits distributed in multiple cavities, Phys. Rev. A **101**, 012337 (2020).

[29] T. Bera, S. Majumder, S. K. Sahu, and V. Singh, Large flux-mediated coupling in hybrid electromechanical system with a transmon qubit, arXiv e-prints , arXiv:2001.05700 (2020), arXiv:2001.05700 [cond-mat.mes-hall].

[30] M. N. Lilly and T. S. Humble, Modeling Noisy Quantum Circuits Using Experimental Characterization, arXiv e-prints , arXiv:2001.15653 (2020), arXiv:2001.08653 [quant-ph].

[31] M. Kjaergaard, M. E. Schwartz, A. Greene, G. O. Samach, A. Bengtsson, M. O'Keeffe, C. M. McNally, J. Braumüller, D. K. Kim, P. Krantz, M. Marvian, A. Melville, B. M. Niedzielski, Y. Sung, R. Winik, J. Yoder, D. Rosenberg, K. Obenland, S. Lloyd, T. P. Orland o, I. Marvian, S. Gustavsson, and W. D. Oliver, A Quantum Instruction Set Implemented on a Superconducting Quantum Processor, arXiv e-prints , arXiv:2001.08838 (2020), arXiv:2001.08838 [quant-ph].

[32] G. P. Fedorov, V. B. Yursa, A. E. Efimov, K. I. Shiianov, A. Y. Dmitriev, I. A. Rodionov, A. A. Dobronosova, D. O. Moskalev, A. A. Pishchimova, E. I. Malevannaya, and O. V. Astafiev, Light dressing of a diatomic superconducting artificial molecule, Phys. Rev. A **102**, 013707 (2020).

[33] T. Chen and Z.-Y. Xue, High-fidelity and Robust Geometric Quantum Gates That Outperform Dynamical Ones, arXiv e-prints , arXiv:2001.05789 (2020), arXiv:2001.05789 [quant-ph].

[34] B. M. Varbanov, F. Battistel, B. M. Tarasinski, V. P. Ostroukh, T. E. O'Brien, L. DiCarlo, and B. M. Terhal, Leakage detection for a transmon-based surface code, arXiv e-prints , arXiv:2002.07119 (2020), arXiv:2002.07119 [quant-ph].

[35] G. Reznik, S. Bagchi, J. Dressel, and L. Vaidman, Footprints of quantum pigeons, Phys. Rev. Research **2**, 023004 (2020).

[36] P. Zhao, P. Xu, D. Lan, J. Chu, X. Tan, H. Yu, and Y. Yu, High-contrast ZZ interaction using superconducting qubits with opposite-sign anharmonicity, arXiv e-prints , arXiv:2002.07560 (2020), arXiv:2002.07560 [quant-ph].

[37] R. K. L. Colmenar, U. Güngördü, and J. P. Kestner, Simulated randomized benchmarking of a dynamically corrected cross-resonance gate, Phys. Rev. A **102**, 032626 (2020).

[38] A. M. Vadiraj, A. Ask, T. G. McConkey, I. Nsanzineza, C. W. Sandbo Chang, A. Frisk Kockum, and C. M. Wilson, Engineering the Level Structure of a Giant Artificial Atom in Waveguide Quantum Electrodynamics, arXiv e-prints , arXiv:2003.14167 (2020), arXiv:2003.14167 [quant-ph].

[39] M. Scigliuzzo, A. Bengtsson, J.-C. Besse, A. Wallraff, P. Delsing, and S. Gasparinetti, Primary thermometry of propagating microwaves in the quantum regime, arXiv e-prints , arXiv:2003.13522 (2020), arXiv:2003.13522 [quant-ph].

[40] D. L. Campbell, Y.-P. Shim, B. Kannan, R. Winik, A. Melville, B. M. Niedzielski, J. L. Yoder, C. Tahan, S. Gustavsson, and W. D. Oliver, Universal non-adiabatic control of small-gap superconducting qubits, arXiv e-prints , arXiv:2003.13154 (2020), arXiv:2003.13154 [quant-ph].

[41] T. Figueiredo Roque, A. A. Clerk, and H. Ribeiro, Engineering Fast High-Fidelity Quantum Operations With Constrained Interactions, arXiv e-prints , arXiv:2003.12096 (2020), arXiv:2003.12096 [quant-ph].

[42] M. Werninghaus, D. J. Egger, F. Roy, S. Machnes, F. K. Wilhelm, and S. Filipp, Leakage reduction in fast superconducting

qubit gates via optimal control, arXiv e-prints , arXiv:2003.05952 (2020), arXiv:2003.05952 [quant-ph].
[43] A. P. M. Place, L. V. H. Rodgers, P. Mundada, B. M. Smitham, M. Fitzpatrick, Z. Leng, A. Premkumar, J. Bryon, S. Sussman, G. Cheng, T. Madhavan, H. K. Babla, B. Jaeck, A. Gyenis, N. Yao, R. J. Cava, N. P. de Leon, and A. A. Houck, New material platform for superconducting transmon qubits with coherence times exceeding 0.3 milliseconds, arXiv e-prints , arXiv:2003.00024 (2020), arXiv:2003.00024 [quant-ph].
[44] X. Guan, Y. Feng, Z.-Y. Xue, G. Chen, and S. Jia, Synthetic gauge field and chiral physics on two-leg superconducting circuits, Phys. Rev. A **102**, 032610 (2020).
[45] J. Avila, E. Prada, P. San-Jose, and R. Aguado, Majorana oscillations and parity crossings in semiconductor-nanowire-based transmon qubits, arXiv e-prints , arXiv:2003.02858 (2020), arXiv:2003.02858 [cond-mat.mes-hall].
[46] J. Ku, X. Xu, M. Brink, D. C. McKay, J. B. Hertzberg, M. H. Ansari, and B. L. T. Plourde, Suppression of Unwanted ZZ Interactions in a Hybrid Two-Qubit System, arXiv e-prints , arXiv:2003.02775 (2020), arXiv:2003.02775 [quant-ph].
[47] J. Avila, E. Prada, P. San-Jose, and R. Aguado, Superconducting islands with semiconductor-nanowire-based topological Josephson junctions, arXiv e-prints , arXiv:2003.02852 (2020), arXiv:2003.02852 [cond-mat.supr-con].
[48] B. Kannan, D. Campbell, F. Vasconcelos, R. Winik, D. Kim, M. Kjaergaard, P. Krantz, A. Melville, B. M. Niedzielski, J. Yoder, T. P. Orlando, S. Gustavsson, and W. D. Oliver, Generating Spatially Entangled Itinerant Photons with Waveguide Quantum Electrodynamics, arXiv e-prints , arXiv:2003.07300 (2020), arXiv:2003.07300 [quant-ph].
[49] M. Malekakhlagh, E. Magesan, and D. C. McKay, First-principles analysis of cross-resonance gate operation, Phys. Rev. A **102**, 042605 (2020).
[50] M. Mirhosseini, A. Sipahigil, M. Kalaee, and O. Painter, Quantum transduction of optical photons from a superconducting qubit, arXiv e-prints , arXiv:2004.04838 (2020), arXiv:2004.04838 [quant-ph].
[51] A. Premkumar, C. Weiland, S. Hwang, B. Jaeck, A. P. M. Place, I. Waluyo, A. Hunt, V. Bisogni, J. Pelliciari, A. Barbour, M. S. Miller, P. Russo, F. Camino, K. Kisslinger, X. Tong, M. S. Hybertsen, A. A. Houck, and I. Jarrige, Microscopic Relaxation Channels in Materials for Superconducting Qubits, arXiv e-prints , arXiv:2004.02908 (2020), arXiv:2004.02908 [physics.app-ph].
[52] M. Florentin Gely, Measuring and controlling radio-frequency quanta with superconducting circuits, arXiv e-prints , arXiv:2004.09153 (2020), arXiv:2004.09153 [quant-ph].
[53] J. Xu, S. Li, T. Chen, and Z.-Y. Xue, Nonadiabatic geometric quantum computation with optimal control on superconducting circuits, Frontiers of Physics **15**, 41503 (2020).
[54] Y. Zhang, T. Huan, R.-g. Zhou, and H. Ian, Ramsey-like spectroscopy of superconducting qubits with dispersive evolution, Phys. Rev. A **102**, 013710 (2020).
[55] R. Dassonneville, R. Assouly, T. Peronnin, P. Rouchon, and B. Huard, Number-resolved photocounter for propagating microwave mode, arXiv e-prints , arXiv:2004.05114 (2020), arXiv:2004.05114 [quant-ph].
[56] A. Noguchi, A. Osada, S. Masuda, S. Kono, K. Heya, S. Piotr Wolski, H. Takahashi, T. Sugiyama, D. Lachance-Quirion, and Y. Nakamura, Fast parametric two-qubit gates with suppressed residual interaction using a parity-violated superconducting qubit, arXiv e-prints , arXiv:2005.02630 (2020), arXiv:2005.02630 [quant-ph].
[57] M. Cattaneo, G. L. Giorgi, S. Maniscalco, G. Sorin Paraoanu, and R. Zambrini, Synchronization and subradiance as signatures of entangling bath between superconducting qubits, arXiv e-prints , arXiv:2005.06229 (2020), arXiv:2005.06229 [quant-ph].
[58] Y. Ma, X. Pan, W. Cai, X. Mu, Y. Xu, L. Hu, W. Wang, H. Wang, Y. P. Song, Z.-B. Yang, S.-B. Zheng, and L. Sun, Manipulating complex hybrid entanglement and testing multipartite Bell inequalities in a superconducting circuit, arXiv e-prints , arXiv:2005.09849 (2020), arXiv:2005.09849 [quant-ph].
[59] D. Sabonis, O. Erlandsson, A. Kringhøj, B. van Heck, T. W. Larsen, I. Petkovic, P. Krogstrup, K. D. Petersson, and C. M. Marcus, Destructive little-parks effect in a full-shell nanowire-based transmon, Phys. Rev. Lett. **125**, 156804 (2020).
[60] T. H. Kyaw, T. Menke, S. Sim, N. P. D. Sawaya, W. D. Oliver, G. Giacomo Guerreschi, and A. Aspuru-Guzik, Quantum computer-aided design: digital quantum simulation of quantum processors, arXiv e-prints , arXiv:2006.03070 (2020), arXiv:2006.03070 [quant-ph].
[61] M. Kervinen, A. Välimaa, J. E. Ramírez-Muñoz, and M. A. Sillanpää, Sideband control of a multimode quantum bulk acoustic system, arXiv e-prints , arXiv:2006.05446 (2020), arXiv:2006.05446 [cond-mat.mes-hall].
[62] S. Krinner, P. Kurpiers, B. Royer, P. Magnard, I. Tsitsilin, J. C. Besse, A. Remm, A. Blais, and A. Wallraff, Demonstration of an All-Microwave Controlled-Phase Gate between Far Detuned Qubits, arXiv e-prints , arXiv:2006.10639 (2020), arXiv:2006.10639 [quant-ph].
[63] J. D. Brehm, A. N. Poddubny, A. Stehli, T. Wolz, H. Rotzinger, and A. V. Ustinov, Waveguide Bandgap Engineering with an Array of Superconducting Qubits, arXiv e-prints , arXiv:2006.03330 (2020), arXiv:2006.03330 [quant-ph].
[64] D. Buterakos, S. Das Sarma, and E. Barnes, Geometrical Formalism for Dynamically Corrected Gates in Multiqubit Systems, arXiv e-prints , arXiv:2008.01168 (2020), arXiv:2008.01168 [quant-ph].
[65] S. Singh, A switching approach for perfect state transfer over a scalable and routing enabled network architecture with superconducting qubits, arXiv e-prints , arXiv:2007.02682 (2020), arXiv:2007.02682 [quant-ph].
[66] S. Indrajeet, H. Wang, M. D. Hutchings, B. G. Taketani, F. K. Wilhelm, M. D. LaHaye, and B. L. T. Plourde, Coupling a Superconducting Qubit to a Left-Handed Metamaterial Resonator, arXiv e-prints , arXiv:2007.10932 (2020), arXiv:2007.10932 [quant-ph].
[67] G. Liu, X. Cao, T. C. Chien, C. Zhou, P. Lu, and M. Hatridge, Noise reduction in qubit readout with a two-mode squeezed interferometer, arXiv e-prints , arXiv:2007.15460 (2020), arXiv:2007.15460 [quant-ph].
[68] A. A. Stepanenko, M. D. Lyubarov, and M. A. Gorlach, Topological states in qubit arrays induced by density-dependent coupling, arXiv e-prints , arXiv:2007.06395 (2020), arXiv:2007.06395 [cond-mat.mes-hall].
[69] J. J. García-Ripoll, A. Ruiz-Chamorro, and E. Torrontegui, Quantum control of frequency tunable transmon superconducting qubits, arXiv e-prints , arXiv:2002.10320 (2020), arXiv:2002.10320 [quant-ph].
[70] V. Negîrneac, H. Ali, N. Muthusubramanian, F. Battistel, R. Sagastizabal, M. S. Moreira, J. F. Marques, W. Vlothuizen, M. Beekman, N. Haider, A. Bruno, and L. DiCarlo, High-fidelity controlled-Z gate with maximal intermediate leakage operating at the speed limit in a superconducting quantum processor, arXiv e-prints , arXiv:2008.07411 (2020), arXiv:2008.07411 [quant-ph].
[71] S. Masuda and K. Koshino, Effects of higher levels of qubits on control of qubit protected by a Josephson quantum filter, arXiv e-prints , arXiv:2008.09980 (2020), arXiv:2008.09980 [quant-ph].
[72] W. D. Kalfus, D. F. Lee, G. J. Ribeill, S. D. Fallek, A. Wagner, B. Donovan, D. Ristè, and T. A. Ohki, High-Fidelity Control of Superconducting Qubits Using Direct Microwave Synthesis in Higher Nyquist Zones, arXiv e-prints , arXiv:2008.02873 (2020), arXiv:2008.02873 [quant-ph].
[73] J. T. Monroe, N. Yunger Halpern, T. Lee, and K. W. Murch, Weak Measurement of Superconducting Qubit Reconciles Incompatible Operators, arXiv e-prints , arXiv:2008.09131 (2020), arXiv:2008.09131 [quant-ph].
[74] D. Willsch, Supercomputer simulations of transmon quantum computers, arXiv e-prints , arXiv:2008.13490 (2020), arXiv:2008.13490 [quant-ph].
[75] R. Zhao, S. Park, T. Zhao, M. Bal, C. R. H. McRae, J. Long, and D. P. Pappas, A merged-element transmon, arXiv e-prints , arXiv:2008.07652 (2020), arXiv:2008.07652 [quant-ph].
[76] P. Magnard, S. Storz, P. Kurpiers, J. Schär, F. Marxer, J. Lütolf, J.-C. Besse, M. Gabureac, K. Reuer, A. Akin, B. Royer, A. Blais, and A. Wallraff, Microwave Quantum Link between Superconducting Circuits Housed in Spatially Separated Cryogenic Systems, arXiv e-prints , arXiv:2008.01642 (2020), arXiv:2008.01642 [quant-ph].
[77] A. Kringhøj, G. W. Winkler, T. W. Larsen, D. Sabonis, O. Erlandsson, P. Krogstrup, B. van Heck, K. D. Petersson, and C. M. Marcus, Andreev Modes from Phase Winding in a Full-shell Nanowire-based Transmon, arXiv e-prints , arXiv:2008.10013 (2020), arXiv:2008.10013 [cond-mat.mes-hall].
[78] E. I. Rosenthal, C. M. F. Schneider, M. Malnou, Z. Zhao, F. Leditzky, B. J. Chapman, W. Wustmann, X. Ma, D. A. Palken, M. F. Zanner, L. R. Vale, G. C. Hilton, J. Gao, G. Smith, G. Kirchmair, and K. W. Lehnert, Efficient and low-backaction quantum measurement using a chip-scale detector, arXiv e-prints , arXiv:2008.03805 (2020), arXiv:2008.03805 [quant-ph].
[79] P. Y. Wen, O. V. Ivakhnenko, M. A. Nakonechnyi, B. Suri, J.-J. Lin, W.-J. Lin, J. C. Chen, S. N. Shevchenko, F. Nori, and I.-C. Hoi, Landau-zener-stückelberg-majorana interferometry of a superconducting qubit in front of a mirror, Phys. Rev. B **102**, 075448 (2020).
[80] W. C. Smith, A. Kou, X. Xiao, U. Vool, and M. H. Devoret, Superconducting circuit protected by two-cooper-pair tunneling,

npj Quantum Information **6**, 8 (2020).
[81] T. Hurant and D. D. Stancil, Asymmetry of CNOT gate operation in superconducting transmon quantum processors using cross-resonance entangling, arXiv e-prints , arXiv:2009.01333 (2020), arXiv:2009.01333 [quant-ph].
[82] A. Dinerstein, C. S. Gorham, and E. F. Dumitrescu, The Hybrid Topological Longitudinal Transmon Qubit, arXiv e-prints , arXiv:2009.12278 (2020), arXiv:2009.12278 [quant-ph].
[83] J. B. Hertzberg, E. J. Zhang, S. Rosenblatt, E. Magesan, J. A. Smolin, J.-B. Yau, V. P. Adiga, M. Sandberg, M. Brink, J. M. Chow, and J. S. Orcutt, Laser-annealing Josephson junctions for yielding scaled-up superconducting quantum processors, arXiv e-prints , arXiv:2009.00781 (2020), arXiv:2009.00781 [quant-ph].
[84] C. Duckering, J. M. Baker, D. I. Schuster, and F. T. Chong, Virtualized Logical Qubits: A 2.5D Architecture for Error-Corrected Quantum Computing, arXiv e-prints , arXiv:2009.01982 (2020), arXiv:2009.01982 [quant-ph].
[85] A. Cervera-Lierta, J. S. Kottmann, and A. Aspuru-Guzik, The Meta-Variational Quantum Eigensolver (Meta-VQE): Learning energy profiles of parameterized Hamiltonians for quantum simulation, arXiv e-prints , arXiv:2009.13545 (2020), arXiv:2009.13545 [quant-ph].
[86] A. Stehli, J. D. Brehm, T. Wolz, P. Baity, S. Danilin, V. Seferai, H. Rotzinger, A. V. Ustinov, and M. Weides, Coherent superconducting qubits from a subtractive junction fabrication process, Applied Physics Letters **117**, 124005 (2020), arXiv:2006.16862 [quant-ph].
[87] Y. Ye, K. Peng, M. Naghiloo, G. Cunningham, and K. P. O'Brien, Engineering Purely Nonlinear Coupling with the Quarton, arXiv e-prints , arXiv:2010.09959 (2020), arXiv:2010.09959 [quant-ph].
[88] A. A. Sokolova, G. P. Fedorov, E. V. Il'ichev, and O. V. Astafiev, Single-atom maser with engineered circuit for population inversion, arXiv e-prints , arXiv:2010.04975 (2020), arXiv:2010.04975 [quant-ph].
[89] K. Kaur, T. Sépulcre, N. Roch, I. Snyman, S. Florens, and S. Bera, Absence of spin-boson quantum phase transition for transmon qubits, arXiv e-prints , arXiv:2010.01016 (2020), arXiv:2010.01016 [cond-mat.mes-hall].
[90] H. Dehmelt, Radiofrequency spectroscopy of stored ions i: Storage**part ii: Spectroscopy is now scheduled to appear in volume v of this series., Advances in Atomic and Molecular Physics, **3**, 53 (1968).
[91] W. Paul, Electromagnetic traps for charged and neutral particles, Rev. Mod. Phys. **62**, 531 (1990).
[92] T. P. Meyrath and D. F. James, Theoretical and numerical studies of the positions of cold trapped ions 10.48550/arxiv.physics/9711023 (1997).
[93] J. Cirac and P. Zoller, A scalable quantum computer with ions in an array of microtraps, Nature **404**, 579 (2000).
[94] D. Kielpinski, C. Monroe, and D. Wineland, Architecture for a large-scale ion-trap quantum computer, Nature **417**, 709 (2002).
[95] U. Tanaka, K. Masuda, Y. Akimoto, K. Koda, Y. Ibaraki, and S. Urabe, Micromotion compensation in a surface electrode trap by parametric excitation of trapped ions, Applied Physics B **107** (2011).
[96] F. Hakelberg, P. Kiefer, M. Wittemer, U. Warring, and T. Schaetz, Interference in a prototype of a two-dimensional ion trap array quantum simulator, Phys. Rev. Lett. **123**, 100504 (2019).
[97] P. Kiefer, F. Hakelberg, M. Wittemer, A. Bermúdez, D. Porras, U. Warring, and T. Schaetz, Floquet-engineered vibrational dynamics in a two-dimensional array of trapped ions, Phys. Rev. Lett. **123**, 213605 (2019).
[98] E. Perego, L. Duca, and C. Sias, Electro-optical ion trap for experiments with atom-ion quantum hybrid systems, arXiv e-prints , arXiv:2001.11968 (2020), arXiv:2001.11968 [physics.atom-ph].
[99] M. Pawlak and H. R. Sadeghpour, Rydberg spectrum of a single trapped ca^{+} ion: A floquet analysis, Phys. Rev. A **101**, 052510 (2020).
[100] G. Higgins, C. Zhang, F. Pokorny, H. Parke, E. Jansson, S. Salim, and M. Hennrich, Observation of effects due to an atom's electric quadrupole polarizability, arXiv e-prints , arXiv:2005.01957 (2020), arXiv:2005.01957 [physics.atom-ph].
[101] L. A. Zhukas, M. J. Millican, P. Svihra, A. Nomerotski, and B. B. Blinov, Direct Observation of Ion Micromotion in a Linear Paul Trap, arXiv e-prints , arXiv:2010.00159 (2020), arXiv:2010.00159 [physics.atom-ph].
[102] M. Ghadimi, A. Zappacosta, J. Scarabel, K. Shimizu, E. W. Streed, and M. Lobino, Dynamic compensation of stray electric fields in an ion trap using machine learning and adaptive algorithm (2021).
[103] J. M. Pino, J. M. Dreiling, C. Figgatt, J. P. Gaebler, S. A. Moses, M. S. Allman, C. H. Baldwin, M. Foss-Feig, D. Hayes, K. Mayer, C. Ryan-Anderson, and B. Neyenhuis, Demonstration of the trapped-ion quantum CCD computer architecture, Nature (London) **592**, 209 (2021), arXiv:2003.01293 [quant-ph].
[104] M. Lee, J. Jeong, Y. Park, C. Jung, T. Kim, and D.-i. Cho, Ion shuttling method for long-range shuttling of trapped ions in MEMS-fabricated ion traps, Japanese Journal of Applied Physics **60**, 027004 (2021).
[105] R. Saito, K. Saito, and T. Mukaiyama, Measurement of ion displacement via RF power variation for excess micromotion compensation, Journal of Applied Physics **129**, 124302 (2021).
[106] Y. Liu, Q.-f. Lao, P.-f. Lu, X.-x. Rao, H. Wu, T. Liu, K.-x. Wang, Z. Wang, M.-s. Li, F. Zhu, and L. Luo, Minimization of the micromotion of trapped ions with artificial neural networks, Applied Physics Letters **119**, 134002 (2021), arXiv:2103.02231 [physics.atom-ph].
[107] Y. H. Teoh, M. Sajjan, Z. Sun, F. Rajabi, and R. Islam, Manipulating phonons of a trapped-ion system using optical tweezers, Physical Review A **104**, 10.1103/physreva.104.022420 (2021).
[108] M.-S. Li, X.-X. Rao, Z. Wang, P.-F. Lu, F. Zhu, Y. Liu, and L. Luo, Homogeneous linear ion crystal in a hybrid potential, Quantum Information Processing **21**, 65 (2022), arXiv:2103.02158 [physics.atom-ph].
[109] M. Siegele-Brown, S. Hong, F. R. Lebrun-Gallagher, S. J. Hile, S. Weidt, and W. K. Hensinger, Fabrication of Surface Ion Traps with Integrated Current Carrying Wires enabling High Magnetic Field Gradients, arXiv e-prints , arXiv:2202.02313 (2022), arXiv:2202.02313 [quant-ph].
[110] T. Lindvall, K. J. Hanhijärvi, T. Fordell, and A. E. Wallin, High-accuracy determination of paul-trap stability parameters for electric-quadrupole-shift prediction, Journal of Applied Physics **132**, 124401 (2022).
[111] W. C. Burton, B. Estey, I. M. Hoffman, A. R. Perry, C. Volin, and G. Price, Transport of multispecies ion crystals through a junction in an rf paul trap (2022).
[112] S. N. Miao, J. W. Zhang, Y. Zheng, H. R. Qin, N. C. Xin, Y. T. Chen, J. Z. Han, and L. J. Wang, Second-order doppler frequency shifts of trapped ions in a linear paul trap (2022).
[113] J. Zhang, B. T. Chow, S. Ejtemaee, and P. C. Haljan, Spectroscopic Characterization of the Quantum Linear-Zigzag Transition in Trapped Ions, arXiv e-prints , arXiv:2206.00490 (2022), arXiv:2206.00490 [quant-ph].
[114] B. M. Mihalcea, Quasienergy operators and generalized squeezed states for systems of trapped ions, Annals of Physics **442**, 168926 (2022), arXiv:2108.11628 [quant-ph].
[115] D. James, Quantum dynamics of cold trapped ions with application to quantum computation, Applied Physics B: Lasers and Optics **66**, 181 (1998).
[116] A. Sørensen and K. Mølmer, Entanglement and quantum computation with ions in thermal motion, Phys. Rev. A **62**, 022311 (2000).
[117] A. Steane, C. F. Roos, D. Stevens, A. Mundt, D. Leibfried, F. Schmidt-Kaler, and R. Blatt, Speed of ion-trap quantum-information processors, Phys. Rev. A **62**, 042305 (2000).
[118] D. Leibfried, B. DeMarco, V. Meyer, D. Lucas, M. Barrett, J. Britton, W. M. Itano, B. Jelenković, C. Langer, T. Rosenband, and D. J. Wineland, Experimental demonstration of a robust, high-fidelity geometric two ion-qubit phase gate, Nature **422**, 412 (2003).
[119] J. J. García-Ripoll, P. Zoller, and J. I. Cirac, Speed optimized two-qubit gates with laser coherent control techniques for ion trap quantum computing, Phys. Rev. Lett. **91**, 157901 (2003).
[120] K. R. Brown, A. C. Wilson, Y. Colombe, C. Ospelkaus, A. M. Meier, E. Knill, D. Leibfried, and D. J. Wineland, Single-qubit-gate error below $\mathbf{10^{-4}}$ in a trapped ion, Phys. Rev. A **84**, 030303 (2011).
[121] T. P. Harty, D. T. C. Allcock, C. J. Ballance, L. Guidoni, H. A. Janacek, N. M. Linke, D. N. Stacey, and D. M. Lucas, High-fidelity preparation, gates, memory, and readout of a trapped-ion quantum bit, Phys. Rev. Lett. **113**, 220501 (2014).
[122] C. J. Ballance, T. P. Harty, N. M. Linke, M. A. Sepiol, and D. M. Lucas, High-fidelity quantum logic gates using trapped-ion hyperfine qubits, Phys. Rev. Lett. **117**, 060504 (2016).
[123] N. M. Linke, D. Maslov, M. Roetteler, S. Debnath, C. Figgatt, K. A. Landsman, K. Wright, and C. Monroe, Experimental comparison of two quantum computing architectures, Proceedings of the National Academy of Sciences **114**, 3305 (2017).
[124] P. H. Leung, K. A. Landsman, C. Figgatt, N. M. Linke, C. Monroe, and K. R. Brown, Robust 2-qubit gates in a linear ion crystal using a frequency-modulated driving force, Phys. Rev. Lett. **120**, 020501 (2018).
[125] P. H. Leung and K. R. Brown, Entangling an arbitrary pair of qubits in a long ion crystal, Phys. Rev. A **98**, 032318 (2018).
[126] N. M. Linke, S. Johri, C. Figgatt, K. A. Landsman, A. Y. Mat-

suura, and C. Monroe, Measuring the rényi entropy of a two-site fermi-hubbard model on a trapped ion quantum computer, Phys. Rev. A **98**, 052334 (2018).
[127] F. Rajabi, S. Motlakunta, C.-Y. Shih, N. Kotibhaskar, Q. Quraishi, A. Ajoy, and R. Islam, Dynamical Hamiltonian engineering of 2D rectangular lattices in a one-dimensional ion chain, npj Quantum Information **5**, 32 (2019), arXiv:1808.06124 [quant-ph].
[128] Y. H. Teoh, M. Drygala, R. G. Melko, and R. Islam, Machine learning design of a trapped-ion quantum spin simulator, Quantum Science and Technology **5**, 024001 (2020), arXiv:1910.02496 [quant-ph].
[129] E. P. G. Gale, Z. Mehdi, L. M. Oberg, A. K. Ratcliffe, S. A. Haine, and J. J. Hope, Optimized fast gates for quantum computing with trapped ions, Phys. Rev. A **101**, 052328 (2020).
[130] P. J. Low, B. M. White, A. A. Cox, M. L. Day, and C. Senko, Practical trapped-ion protocols for universal qudit-based quantum computing, Phys. Rev. Research **2**, 033128 (2020).
[131] M. W. van Mourik, E. A. Martinez, L. Gerster, P. Hrmo, T. Monz, P. Schindler, and R. Blatt, Coherent rotations of qubits within a surface ion-trap quantum computer, Phys. Rev. A **102**, 022611 (2020), arXiv:2001.02440 [quant-ph].
[132] Y. K. Wu, Z. D. Liu, W. D. Zhao, and L. M. Duan, High Fidelity Entangling Gates in a 3D Ion Crystal under Micromotion, arXiv e-prints , arXiv:2009.13007 (2020), arXiv:2009.13007 [quant-ph].
[133] E. Torrontegui, D. Heinrich, M. I. Hussain, R. Blatt, and J. J. García-Ripoll, Ultra-fast two-qubit ion gate using sequences of resonant pulses, New Journal of Physics **22**, 103024 (2020).
[134] C. Monroe, W. C. Campbell, L.-M. Duan, Z.-X. Gong, A. V. Gorshkov, P. W. Hess, R. Islam, K. Kim, N. M. Linke, G. Pagano, P. Richerme, C. Senko, and N. Y. Yao, Programmable quantum simulations of spin systems with trapped ions, Rev. Mod. Phys. **93**, 025001 (2021).
[135] I. Pogorelov, T. Feldker, C. D. Marciniak, L. Postler, G. Jacob, O. Krieglsteiner, V. Podlesnic, M. Meth, V. Negnevitsky, M. Stadler, B. Höfer, C. Wächter, K. Lakhmanskiy, R. Blatt, P. Schindler, and T. Monz, Compact Ion-Trap Quantum Computing Demonstrator, PRX Quantum **2**, 020343 (2021), arXiv:2101.11390 [quant-ph].
[136] R. T. Sutherland and R. Srinivas, Universal hybrid quantum computing in trapped ions, Physical Review A **104**, 10.1103/physreva.104.032609 (2021).
[137] K. Shimizu, J. Scarabel, E. Bridge, S. Connell, M. Ghadimi, B. Haylock, M. I. Hussain, E. Streed, and M. Lobino, Ultrafast coherent excitation of an ytterbium ion with single laser pulses, Applied Physics Letters **119**, 214003 (2021), arXiv:2109.13523 [quant-ph].
[138] M. L. Day, P. J. Low, B. White, R. Islam, and C. Senko, Limits on atomic qubit control from laser noise, npj Quantum Information **8**, 72 (2022), arXiv:2112.04946 [quant-ph].
[139] R. T. Sutherland, Q. Yu, K. M. Beck, and H. Häffner, One- and two-qubit gate infidelities due to motional errors in trapped ions and electrons, Phys. Rev. A **105**, 022437 (2022).
[140] F. Martínez-García, L. Gerster, D. Vodola, P. Hrmo, T. Monz, P. Schindler, and M. Müller, Analytical and experimental study of center-line miscalibrations in mølmer-sørensen gates, Phys. Rev. A **105**, 032437 (2022).
[141] L. M. Duan, Robust gate design for large ion crystals through excitation of local phonon modes (2022).
[142] R. T. Sutherland, R. Srinivas, and D. T. C. Allcock, Individual addressing of trapped ion qubits with geometric phase gates (2022).
[143] D. Yum and T. Choi, Progress of quantum entanglement in a trapped-ion based quantum computer, Current Applied Physics **41**, 163 (2022).
[144] W. R. Hamilton, Xv. on a general method in dynamics; by which the study of the motions of all free systems of attracting or repelling points is reduced to the search and differentiation of one central relation, or characteristic function, Philosophical Transactions of the Royal Society of London **124**, 247 (1834).
[145] W. R. Hamilton, Vii. second essay on a general method in dynamics, Philosophical Transactions of the Royal Society of London **125**, 95 (1835).
[146] E. Schrödinger, An undulatory theory of the mechanics of atoms and molecules, Phys. Rev. **28**, 1049 (1926).
[147] C. de Coulomb, Memoirs on electricity and magnetism 10.5479/sil.304245.39088000647479 (1789).
[148] J. Lagrange, Works of Lagrange, (1777).
[149] I. Kovacic, R. Rand, and S. Mohamed Sah, Mathieu's Equation and Its Generalizations: Overview of Stability Charts and Their Features, Applied Mechanics Reviews **70**, 10.1115/1.4039144 (2018), 020802.
[150] D. J. Daniel, Exact solutions of Mathieu's equation, Progress of Theoretical and Experimental Physics **2020**, 043A01 (2020).
[151] D. P. Nadlinger, P. Drmota, D. Main, B. C. Nichol, G. Araneda, R. Srinivas, L. J. Stephenson, C. J. Ballance, and D. M. Lucas, Micromotion minimisation by synchronous detection of parametrically excited motion (2021).
[152] F. E. Neumann, General laws of induced electric currents, Annalen der Physik **143**, 31 (1846).
[153] W. Pauli, On the quantum mechanics of the magnetic electron, Zeitschrift fur Physik **43**, 601 (1927).
[154] J. C. Slater and G. F. Koster, Simplified lcao method for the periodic potential problem, Phys. Rev. **94**, 1498 (1954).
[155] G. Lüders, About the change of state through the measurement process, Annalen der Physik **443**, 322 (2006).
[156] R. Islam, Quantum simulation of interacting spin models with trapped ions, (2012).
[157] G. N. Nop, D. Paudyal, and J. D. H. Smith, Ytterbium ion trap quantum computing: The current state-of-the-art, AVS Quantum Science **3**, 044101 (2021).
[158] W. Pauli, On the connection between the termination of the electron groups in the atom and the complex structure of the spectra, Zeitschrift für Physik 10.1007/BF02980631 (1925).
[159] A. R. Brown and L. Susskind, Second law of quantum complexity, Phys. Rev. D **97**, 086015 (2018).
[160] R. M. N. Pesce and P. D. Stevenson, H2zixy: Pauli spin matrix decomposition of real symmetric matrices (2021).
[161] J. L. R. d'Alembert, *Treatise on dynamics* (1743).
[162] J.-L. Lagrange, *Solution of Different Problems of Integral Calculation* (1867) pp. 469 – 668.
[163] P. A. M. Dirac, *The Principles of Quantum Mechanics* (Clarendon Press, 1930).
[164] K. Saito, R. Saito, and T. Mukaiyama, Ion trap frequency measurement from fluorescence dynamics, Journal of Applied Physics **132**, 094401 (2022).
[165] D. P. DiVincenzo, The physical implementation of quantum computation, Fortschritte der Physik **48**, 771 (2000).
[166] A. M. Childs, J. Leng, T. Li, J.-P. Liu, and C. Zhang, Quantum simulation of real-space dynamics (2022).
[167] S. Lloyd, Universal quantum simulators, Science **273**, 1073 (1996).
[168] Y. I. Manin, Computable and uncomputable, Sovetskoye Radio, Moscow (1980).
[169] T. Kato, On the trotter-lie product formula, Proceedings of The Japan Academy **50** (1974).
[170] M. Lapidus, Generalization of the trotter-lie formula, Integral Equations and Operator Theory **4**, 366 (1981).
[171] D. Aharonov and A. Ta-Shma, Adiabatic Quantum State Generation and Statistical Zero Knowledge, arXiv e-prints , quant-ph/0301023 (2003), arXiv:quant-ph/0301023 [quant-ph].
[172] D. W. Berry, G. Ahokas, R. Cleve, and B. C. Sanders, Efficient quantum algorithms for simulating sparse hamiltonians, Communications in Mathematical Physics **270**, 359 (2006).
[173] A. W. Harrow, A. Hassidim, and S. Lloyd, Quantum algorithm for linear systems of equations, Physical Review Letters **103**, 10.1103/physrevlett.103.150502 (2009).
[174] A. M. Childs, On the relationship between continuous- and discrete-time quantum walk, Communications in Mathematical Physics **294**, 581 (2009).
[175] A. M. Childs and R. Kothari, Simulating sparse hamiltonians with star decompositions, in *Theory of Quantum Computation, Communication, and Cryptography* (Springer Berlin Heidelberg, 2011) pp. 94–103.
[176] B. C. Sanders, Efficient algorithms for universal quantum simulation, in *Reversible Computation* (Springer Berlin Heidelberg, 2013) pp. 1–10.
[177] I. Georgescu, S. Ashhab, and F. Nori, Quantum simulation, Reviews of Modern Physics **86**, 153 (2014).
[178] S. Hadfield and A. Papageorgiou, Divide and conquer approach to quantum hamiltonian simulation, New Journal of Physics **20**, 043003 (2018).
[179] A. M. Childs, D. Maslov, Y. Nam, N. J. Ross, and Y. Su, Toward the first quantum simulation with quantum speedup, Proceedings of the National Academy of Sciences **115**, 9456 (2018).
[180] E. Campbell, Random compiler for fast hamiltonian simulation, Phys. Rev. Lett. **123**, 070503 (2019).
[181] A. M. Childs and Y. Su, Nearly optimal lattice simulation by product formulas, Phys. Rev. Lett. **123**, 050503 (2019).
[182] A. M. Childs, A. Ostrander, and Y. Su, Faster quantum simulation by randomization, Quantum **3**, 182 (2019).
[183] A. M. Childs, Y. Su, M. C. Tran, N. Wiebe, and S. Zhu, A Theory of Trotter Error, arXiv e-prints , arXiv:1912.08854 (2019), arXiv:1912.08854 [quant-ph].
[184] Y. Ouyang, D. R. White, and E. T. Campbell, Compilation by stochastic Hamiltonian sparsification, Quantum **4**, 235 (2020).

[185] M. C. Tran, S.-K. Chu, Y. Su, A. M. Childs, and A. V. Gorshkov, Destructive Error Interference in Product-Formula Lattice Simulation, Phys. Rev. Lett. **124**, 220502 (2020), arXiv:1912.11047 [quant-ph].

[186] M. C. Tran, Y. Su, D. Carney, and J. M. Taylor, Faster digital quantum simulation by symmetry protection, PRX Quantum **2**, 10.1103/prxquantum.2.010323 (2021).

[187] L. Zhou and D. Aharonov, Strongly universal hamiltonian simulators (2021).

[188] L. Clinton, J. Bausch, and T. Cubitt, Hamiltonian simulation algorithms for near-term quantum hardware, Nature Communications **12**, 10.1038/s41467-021-25196-0 (2021).

[189] A. M. Childs, Y. Su, M. C. Tran, N. Wiebe, and S. Zhu, Theory of trotter error with commutator scaling, Phys. Rev. X **11**, 011020 (2021).

[190] C. Kargi, J. P. Dehollain, F. Henriques, L. M. Sieberer, T. Olsacher, P. Hauke, M. Heyl, P. Zoller, and N. K. Langford, Quantum chaos and universal trotterisation behaviours in digital quantum simulations (2021).

[191] D. Burgarth, N. Galke, A. Hahn, and L. van Luijk, State-dependent trotter limits and their approximations (2022).

[192] G. Burkard, Recipes for the digital quantum simulation of lattice spin systems (2022).

[193] K. Mizuta and K. Fujii, Optimal time-periodic Hamiltonian simulation with Floquet-Hilbert space, arXiv e-prints , arXiv:2209.05048 (2022), arXiv:2209.05048 [quant-ph].

[194] G. Vidal, Efficient simulation of one-dimensional quantum many-body systems, Physical Review Letters **93**, 10.1103/physrevlett.93.040502 (2004).

[195] F. Verstraete, J. J. García-Ripoll, and J. I. Cirac, Matrix product density operators: Simulation of finite-temperature and dissipative systems, Physical Review Letters **93**, 10.1103/physrevlett.93.207204 (2004).

[196] I. Buluta and F. Nori, Quantum simulators, Science **326**, 108 (2009).

[197] B. P. Lanyon, J. D. Whitfield, G. G. Gillett, M. E. Goggin, M. P. Almeida, I. Kassal, J. D. Biamonte, M. Mohseni, B. J. Powell, M. Barbieri, A. Aspuru-Guzik, and A. G. White, Towards quantum chemistry on a quantum computer, Nature Chemistry **2**, 106 (2010).

[198] B. P. Lanyon, C. Hempel, D. Nigg, M. Müller, R. Gerritsma, F. Zähringer, P. Schindler, J. T. Barreiro, M. Rambach, G. Kirchmair, M. Hennrich, P. Zoller, R. Blatt, and C. F. Roos, Universal digital quantum simulation with trapped ions, Science **334**, 57 (2011).

[199] D. Wecker, B. Bauer, B. K. Clark, M. B. Hastings, and M. Troyer, Gate-count estimates for performing quantum chemistry on small quantum computers, Physical Review A **90**, 10.1103/physreva.90.022305 (2014).

[200] D. Poulin, M. B. Hastings, D. Wecker, N. Wiebe, A. C. Doherty, and M. Troyer, The trotter step size required for accurate quantum simulation of quantum chemistry 10.48550/ARXIV.1406.4920 (2014).

[201] Y. Salathé, M. Mondal, M. Oppliger, J. Heinsoo, P. Kurpiers, A. Potočnik, A. Mezzacapo, U. Las Heras, L. Lamata, E. Solano, S. Filipp, and A. Wallraff, Digital quantum simulation of spin models with circuit quantum electrodynamics, Phys. Rev. X **5**, 021027 (2015).

[202] Y. Cao, J. Romero, J. P. Olson, M. Degroote, P. D. Johnson, M. Kieferová, I. D. Kivlichan, T. Menke, B. Peropadre, N. P. D. Sawaya, S. Sim, L. Veis, and A. Aspuru-Guzik, Quantum chemistry in the age of quantum computing, Chemical Reviews **119**, 10856 (2019).

[203] E. Gustafson, Y. Meurice, and J. Unmuth-Yockey, Quantum simulation of scattering in the quantum ising model, Phys. Rev. D **99**, 094503 (2019).

[204] A. Smith, M. Kim, F. Pollmann, and J. Knolle, Simulating quantum many-body dynamics on a current digital quantum computer, npj Quantum Information **5** (2019).

[205] S. McArdle, S. Endo, A. Aspuru-Guzik, S. C. Benjamin, and X. Yuan, Quantum computational chemistry, Reviews of Modern Physics **92**, 10.1103/revmodphys.92.015003 (2020).

[206] L. Clinton, J. Bausch, and T. Cubitt, Hamiltonian simulation algorithms for near-term quantum hardware, Nature Communications **12**, 10.1038/s41467-021-25196-0 (2021).

[207] N. Keenan, N. Robertson, T. Murphy, S. Zhuk, and J. Goold, Evidence of kardar-parisi-zhang scaling on a digital quantum simulator (2022).

[208] S. Raeisi, N. Wiebe, and B. C. Sanders, Quantum-circuit design for efficient simulations of many-body quantum dynamics, New Journal of Physics **14**, 103017 (2012), arXiv:1108.4318 [quant-ph].

[209] R. Babbush, N. Wiebe, J. McClean, J. McClain, H. Neven, and G. K.-L. Chan, Low-depth quantum simulation of materials, Phys. Rev. X **8**, 011044 (2018).

[210] F. Tacchino, A. Chiesa, S. Carretta, and D. Gerace, Quantum computers as universal quantum simulators: State-of-the-art and perspectives, Advanced Quantum Technologies **3**, 1900052 (2019).

[211] K. Bharti, A. Cervera-Lierta, T. H. Kyaw, T. Haug, S. Alperin-Lea, A. Anand, M. Degroote, H. Heimonen, J. S. Kottmann, T. Menke, W.-K. Mok, S. Sim, L.-C. Kwek, and A. Aspuru-Guzik, Noisy intermediate-scale quantum algorithms, Reviews of Modern Physics **94**, 10.1103/revmodphys.94.015004 (2022).

[212] Q. Miao and T. Barthel, A quantum-classical eigensolver using multiscale entanglement renormalization, arXiv e-prints , arXiv:2108.13401 (2021), arXiv:2108.13401 [quant-ph].

[213] O. Shehab, K. A. Landsman, Y. Nam, D. Zhu, N. M. Linke, M. J. Keesan, R. C. Pooser, and C. R. Monroe, Toward convergence of effective field theory simulations on digital quantum computers, arXiv e-prints , arXiv:1904.04338 (2019), arXiv:1904.04338 [quant-ph].

[214] Y. Yang, J. I. Cirac, and M. C. Bañuls, Classical algorithms for many-body quantum systems at finite energies, Physical Review B **106**, 10.1103/physrevb.106.024307 (2022).

[215] L. Clinton, T. Cubitt, B. Flynn, F. M. Gambetta, J. Klassen, A. Montanaro, S. Piddock, R. A. Santos, and E. Sheridan, Towards near-term quantum simulation of materials (2022).

[216] S. Flannigan, N. Pearson, G. H. Low, A. Buyskikh, I. Bloch, P. Zoller, M. Troyer, and A. J. Daley, Propagation of errors and quantitative quantum simulation with quantum advantage (2022).

[217] S. P. Jordan, K. S. M. Lee, and J. Preskill, Quantum algorithms for quantum field theories, Science **336**, 1130 (2012).

[218] D. B. Kaplan, N. Klco, and A. Roggero, Ground states via spectral combing on a quantum computer (2017).

[219] N. Klco, E. F. Dumitrescu, A. J. McCaskey, T. D. Morris, R. C. Pooser, M. Sanz, E. Solano, P. Lougovski, and M. J. Savage, Quantum-classical computation of schwinger model dynamics using quantum computers, Physical Review A **98**, 10.1103/physreva.98.032331 (2018).

[220] N. Klco and M. J. Savage, Digitization of scalar fields for quantum computing, Physical Review A **99**, 10.1103/physreva.99.052335 (2019).

[221] N. Klco and M. J. Savage, Minimally entangled state preparation of localized wave functions on quantum computers, Physical Review A **102**, 10.1103/physreva.102.012612 (2020).

[222] N. Klco, M. J. Savage, and J. R. Stryker, SU(2) non-abelian gauge field theory in one dimension on digital quantum computers, Physical Review D **101**, 10.1103/physrevd.101.074512 (2020).

[223] H. Lamm, S. Lawrence, and Y. Yamauchi, Parton physics on a quantum computer, Physical Review Research **2**, 10.1103/physrevresearch.2.013272 (2020).

[224] H. Lamm, S. Lawrence, and Y. Yamauchi, Suppressing coherent gauge drift in quantum simulations (2020).

[225] M. C. Bañuls, R. Blatt, J. Catani, A. Celi, J. I. Cirac, M. Dalmonte, L. Fallani, K. Jansen, M. Lewenstein, S. Montangero, C. A. Muschik, B. Reznik, E. Rico, L. Tagliacozzo, K. V. Acoleyen, F. Verstraete, U.-J. Wiese, M. Wingate, J. Zakrzewski, and P. Zoller, Simulating lattice gauge theories within quantum technologies, The European Physical Journal D **74**, 10.1140/epjd/e2020-100571-8 (2020).

[226] N. H. Nguyen, M. C. Tran, Y. Zhu, A. M. Green, C. H. Alderete, Z. Davoudi, and N. M. Linke, Digital quantum simulation of the schwinger model and symmetry protection with trapped ions (2021).

[227] J. C. Halimeh, H. Lang, J. Mildenberger, Z. Jiang, and P. Hauke, Gauge-symmetry protection using single-body terms, PRX Quantum **2**, 10.1103/prxquantum.2.040311 (2021).

[228] T. Bhattacharya, A. J. Buser, S. Chandrasekharan, R. Gupta, and H. Singh, Qubit regularization of asymptotic freedom, Phys. Rev. Lett. **126**, 172001 (2021).

[229] A. Ciavarella, N. Klco, and M. J. Savage, Trailhead for quantum simulation of su(3) yang-mills lattice gauge theory in the local multiplet basis, Phys. Rev. D **103**, 094501 (2021).

[230] A. Kan and Y. Nam, Lattice quantum chromodynamics and electrodynamics on a universal quantum computer (2021).

[231] M. Carena, H. Lamm, Y.-Y. Li, and W. Liu, Improved hamiltonians for quantum simulations of gauge theories, Phys. Rev. Lett. **129**, 051601 (2022).

[232] E. Whittaker, On the functions which are represented by the expansions of the interpolation theory, Proceedings of the Royal Society of Edinburgh **35**, 181 (1915).

[233] H. Nyquist, Certain topics in telegraph transmission theory, Transactions of the American Institute of Electrical Engineers **47**, 617 (1928).

[234] C. Shannon, Communication in the presence of noise, Proceedings

of the IRE **37**, 10 (1949).
[235] J. A. Oteo, The baker-campbell-hausdorff formula and nested commutator identities, Journal of Mathematical Physics **32**, 419 (1991).
[236] M. Sipser, *Introduction to the Theory of Computation* (Cengage Learning, 2006).
[237] D. W. Berry, A. M. Childs, R. Cleve, R. Kothari, and R. D. Somma, Simulating hamiltonian dynamics with a truncated taylor series, Physical Review Letters **114**, 10.1103/physrevlett.114.090502 (2015).
[238] G. Floquet, On linear differential equations with periodic coefficients, Annales scientifiques de l'École Normale Supérieure **2e série, 12**, 47 (1883).
[239] V. M. Bastidas, T. Haug, C. Gravel, L.-C. Kwek, W. J. Munro, and K. Nemoto, Stroboscopic hamiltonian engineering in the low-frequency regime with a one-dimensional quantum processor, Physical Review B **105**, 10.1103/physrevb.105.075140 (2022).
[240] R. Ineichen, Leibniz, caramul, harriot and the dual system, Mitteilungen der Deutschen Mathematiker-Vereinigung **16**, 12 (2008).
[241] T. Santhanam and A. Tekumalla, Quantum mechanics in finite dimensions. [position and momentum operator commutators, heisenberg relation], Found. Phys. (1976).
[242] R. Jagannathan, T. Santhanam, and R. Vasudevan, Finite-dimensional quantum mechanics of a particle, International Journal of Theoretical Physics **20**, 755 (1981).
[243] S. Gudder and V. Naroditsky, Finite-dimensional quantum mechanics, International Journal of Theoretical Physics **20**, 619 (1981).
[244] A. C. de la Torre and D. Goyeneche, Quantum mechanics in finite-dimensional hilbert space, American Journal of Physics **71**, 49 (2003).
[245] N. Cotfas, J.-P. Gazeau, and A. Vourdas, Finite-dimensional hilbert space and frame quantization, Journal of Physics A: Mathematical and Theoretical **44**, 175303 (2011).
[246] E. Pisanty and E. Nahmad-Achar, On the spectrum of field quadratures for a finite number of photons, Journal of Physics A: Mathematical and Theoretical **45**, 395303 (2012).
[247] Z. Davoudi, I. Raychowdhury, and A. Shaw, Search for efficient formulations for hamiltonian simulation of non-abelian lattice gauge theories, Phys. Rev. D **104**, 074505 (2021).
[248] A. Macridin, A. C. Y. Li, S. Mrenna, and P. Spentzouris, Bosonic field digitization for quantum computers, Physical Review A **105**, 10.1103/physreva.105.052405 (2022).
[249] P. J. Bardroff, C. Leichtle, G. Schrade, and W. P. Schleich, Endoscopy in the paul trap: Measurement of the vibratory quantum state of a single ion, Phys. Rev. Lett. **77**, 2198 (1996).
[250] C. McKee, Apple's M1 Max 14-inch MacBook Pro with 64GB RAM is in stock, 200 dollars off (2022).
[251] Mac Pro Actual Maximum RAM (2022).
[252] C. Choi, The Beating Heart of the World's First Exascale Supercomputer (2022).
[253] G. Fubini, On the metrics defined by a hermitian form, Office graf. C. Ferrari (1904).
[254] E. Study, Shortest routes in a complex area, Mathematische Annalen **60**, 321 (1905).
[255] A. Haar, The standard in the theory of continuous groups, Annals of Mathematics **34**, 147 (1933).
[256] L. J. Boya, E. Sudarshan, and T. Tilma, Volumes of compact manifolds, Reports on Mathematical Physics **52**, 401 (2003).
[257] Andrew Shaw, Universalizing analog quantum simulators 10.48550/arxiv.2203.17249 (2022).
[258] M.-D. Choi, Completely positive linear maps on complex matrices, Linear Algebra and its Applications **10**, 285 (1975).
[259] K. Kraus, A. Böhm, J. D. Dollard, and W. H. Wootters, *States, Effects, and Operations Fundamental Notions of Quantum Theory*, Vol. 190 (1983).
[260] J. Preskill, Quantum information notes: Foundations of quantum theory ii: Measurement and evolution, October, 2018 ().
[261] J. v. Neumann, Probabilistic theory of quantum mechanics, Nachrichten von der Gesellschaft der Wissenschaften zu Göttingen, Mathematisch-Physikalische Klasse **1927**, 245 (1927).
[262] L. Landau, The damping problem in quantum mechanics, in *Collected Papers of L.D. Landau* (Pergamon, 1927) Chap. 2, pp. 8–18.
[263] M. A. Nielsen, A simple formula for the average gate fidelity of a quantum dynamical operation, Physics Letters A **303**, 249 (2002).
[264] Andrew Shaw, Classical-quantum noise mitigation for nisq hardware (2021).
[265] J. Emerson, R. Alicki, and K. Życzkowski, Scalable noise estimation with random unitary operators, Journal of Optics B: Quantum and Semiclassical Optics **7**, S347 (2005).
[266] B. Lé vi, C. C. López, J. Emerson, and D. G. Cory, Efficient error characterization in quantum information processing, Physical Review A **75**, 10.1103/physreva.75.022314 (2007).
[267] C. Dankert, R. Cleve, J. Emerson, and E. Livine, Exact and approximate unitary 2-designs and their application to fidelity estimation, Physical Review A **80**, 10.1103/physreva.80.012304 (2009).
[268] E. Knill, D. Leibfried, R. Reichle, J. Britton, R. B. Blakestad, J. D. Jost, C. Langer, R. Ozeri, S. Seidelin, and D. J. Wineland, Randomized benchmarking of quantum gates, Physical Review A **77**, 10.1103/physreva.77.012307 (2008).
[269] E. Magesan, J. M. Gambetta, and J. Emerson, Scalable and robust randomized benchmarking of quantum processes, Physical Review Letters **106**, 10.1103/physrevlett.106.180504 (2011).
[270] E. Magesan, R. Blume-Kohout, and J. Emerson, Gate fidelity fluctuations and quantum process invariants, Physical Review A **84**, 10.1103/physreva.84.012309 (2011).
[271] E. Magesan, J. M. Gambetta, and J. Emerson, Characterizing quantum gates via randomized benchmarking, Physical Review A **85**, 10.1103/physreva.85.042311 (2012).
[272] J. Helsen, X. Xue, L. M. K. Vandersypen, and S. Wehner, A new class of efficient randomized benchmarking protocols (2018).
[273] K. Boone, A. Carignan-Dugas, J. J. Wallman, and J. Emerson, Randomized benchmarking under different gate sets, Phys. Rev. A **99**, 032329 (2019), arXiv:1811.01920 [quant-ph].
[274] R. Harper, I. Hincks, C. Ferrie, S. T. Flammia, and J. J. Wallman, Statistical analysis of randomized benchmarking, pra **99**, 052350 (2019).
[275] C. D. Bruzewicz, J. Chiaverini, R. McConnell, and J. M. Sage, Trapped-ion quantum computing: Progress and challenges, Applied Physics Reviews **6**, 021314 (2019).
[276] T. J. Proctor, A. Carignan-Dugas, K. Rudinger, E. Nielsen, R. Blume-Kohout, and K. Young, Direct Randomized Benchmarking for Multiqubit Devices, Phys. Rev. Lett. **123**, 030503 (2019), arXiv:1807.07975 [quant-ph].
[277] A. Erhard, J. J. Wallman, L. Postler, M. Meth, R. Stricker, E. A. Martinez, P. Schindler, T. Monz, J. Emerson, and R. Blatt, Characterizing large-scale quantum computers via cycle benchmarking, Nature Communications **10**, 10.1038/s41467-019-13068-7 (2019).
[278] S. T. Flammia and J. J. Wallman, Efficient estimation of pauli channels, ACM Transactions on Quantum Computing **1**, 1 (2020).
[279] E. Onorati, A. Werner, and J. Eisert, Randomized Benchmarking for Individual Quantum Gates, Phys. Rev. Lett. **123**, 060501 (2019), arXiv:1811.11775 [quant-ph].
[280] J. Helsen, X. Xue, L. M. K. Vandersypen, and S. Wehner, A new class of efficient randomized benchmarking protocols, npj Quantum Information **5**, 71 (2019), arXiv:1806.02048 [quant-ph].
[281] E. Derbyshire, J. Y. Malo, A. J. Daley, E. Kashefi, and P. Wallden, Randomized benchmarking in the analogue setting, Quantum Science and Technology **5**, 034001 (2020), arXiv:1909.01295 [quant-ph].
[282] R. Colmenar, U. Güngördü, and J. Kestner, Simulated randomized benchmarking of a dynamically corrected cross-resonance gate, pra **102**, 032626 (2020), arXiv:2002.11802 [quant-ph].
[283] J. Miguel-Ramiro, A. Pirker, and W. Dür, Coherent randomized benchmarking, Physical Review Research **3**, 033038 (2021), arXiv:2010.13810 [quant-ph].
[284] Y. Nakata, D. Zhao, T. Okuda, E. Bannai, Y. Suzuki, S. Tamiya, K. Heya, Z. Yan, K. Zuo, S. Tamate, Y. Tabuchi, and Y. Nakamura, Quantum Circuits for Exact Unitary t -Designs and Applications to Higher-Order Randomized Benchmarking, PRX Quantum **2**, 030339 (2021), arXiv:2102.12617 [quant-ph].
[285] M. Kononenko, M. A. Yurtalan, S. Ren, J. Shi, S. Ashhab, and A. Lupascu, Characterization of control in a superconducting qutrit using randomized benchmarking, Physical Review Research **3**, L042007 (2021), arXiv:2009.00599 [quant-ph].
[286] P. Figueroa-Romero, K. Modi, R. J. Harris, T. M. Stace, and M.-H. Hsieh, Randomized Benchmarking for Non-Markovian Noise, PRX Quantum **2**, 040351 (2021), arXiv:2107.05403 [quant-ph].
[287] K. Yeter-Aydeniz, Z. Parks, A. Nair, E. Gustafson, A. F. Kemper, R. C. Pooser, Y. Meurice, and P. Dreher, Measuring nisq gate-based qubit stability using a 1+1 field theory and cycle benchmarking (2022).
[288] M.-Y. Chen, C. Zhang, and Z.-Y. Xue, Fast high-fidelity geometric gates for singlet-triplet qubits, Physical Review A **105**, 10.1103/physreva.105.022620 (2022).
[289] L. Gerster, F. Martínez-García, P. Hrmo, M. W. van Mourik, B. Wilhelm, D. Vodola, M. Müller, R. Blatt, P. Schindler, and T. Monz, Experimental bayesian calibration of trapped-ion entangling operations, PRX Quantum **3**, 10.1103/prxquantum.3.020350 (2022).
[290] J. Helsen, I. Roth, E. Onorati, A. Werner, and J. Eisert, Gen-

eral framework for randomized benchmarking, PRX Quantum **3**, 020357 (2022).
[291] K. Dubovitskii and Y. Makhlin, Partial randomized benchmarking, Scientific Reports **12**, 10129 (2022), arXiv:2111.04192 [quant-ph].
[292] K. Maruyoshi, T. Okuda, J. W. Pedersen, R. Suzuki, M. Yamazaki, and Y. Yoshida, Conserved charges in the quantum simulation of integrable spin chains, arXiv e-prints , arXiv:2208.00576 (2022), arXiv:2208.00576 [quant-ph].
[293] T. W. Hansch and A. L. Schawlow, Cooling of gases by laser radiation, Optics Communications **13**, 68 (1975).
[294] D. J. Wineland, R. E. Drullinger, and F. L. Walls, Radiation-pressure cooling of bound resonant absorbers, Phys. Rev. Lett. **40**, 1639 (1978).
[295] W. Neuhauser, M. Hohenstatt, P. Toschek, and H. Dehmelt, Optical-sideband cooling of visible atom cloud confined in parabolic well, Phys. Rev. Lett. **41**, 233 (1978).
[296] F. Diedrich, J. C. Bergquist, W. M. Itano, and D. J. Wineland, Laser cooling to the zero-point energy of motion, Phys. Rev. Lett. **62**, 403 (1989).
[297] C. Monroe, D. M. Meekhof, B. E. King, S. R. Jefferts, W. M. Itano, D. J. Wineland, and P. Gould, Resolved-sideband raman cooling of a bound atom to the 3d zero-point energy, Phys. Rev. Lett. **75**, 4011 (1995).
[298] P. Bowe, L. Hornekær, C. Brodersen, M. Drewsen, J. S. Hangst, and J. P. Schiffer, Sympathetic crystallization of trapped ions, Phys. Rev. Lett. **82**, 2071 (1999).
[299] J. Eschner, G. Morigi, F. Schmidt-Kaler, and R. Blatt, Laser cooling of trapped ions, J. Opt. Soc. Am. B **20**, 1003 (2003).
[300] L. González-Sánchez, R. Wester, and F. A. Gianturco, Collisional cooling of internal rotation in MgH^+ ions trapped with He atoms: Quantum modeling meets experiments in Coulomb crystals, Phys. Rev. A **98**, 053423 (2018), arXiv:2010.14458 [physics.atom-ph].
[301] Y. N. Zuo, J. Z. Han, J. W. Zhang, and L. J. Wang, Direct temperature determination of a sympathetically cooled large cd^+ ion crystal for a microwave clock, Applied Physics Letters **115**, 061103 (2019).
[302] K. Blaum, S. Eliseev, and S. Sturm, Perspectives on testing fundamental physics with highly charged ions in penning traps, Quantum Science and Technology **6**, 014002 (2020).
[303] K. Sosnova, A. Carter, and C. Monroe, Character of motional modes for entanglement and sympathetic cooling of mixed-species trapped-ion chains, Physical Review A **103**, 10.1103/physreva.103.012610 (2021).
[304] P. Zhao, J. P. Likforman, H. Y. Li, J. Tao, T. Henner, Y. D. Lim, W. W. Seit, C. S. Tan, and L. Guidoni, TSV-integrated surface electrode ion trap for scalable quantum information processing, Applied Physics Letters **118**, 124003 (2021).
[305] S. Zhang, J.-Q. Zhang, W. Wu, W.-S. Bao, and C. Guo, Fast cooling of trapped ion in strong sideband coupling regime, New Journal of Physics **23**, 023018 (2021).
[306] B. Tu, F. Hahne, I. Arapoglou, A. Egl, F. Heiße, M. Höcker, C. König, J. Morgner, T. Sailer, A. Weigel, R. Wolf, and S. Sturm, Tank-Circuit Assisted Coupling Method for Sympathetic Laser Cooling, arXiv e-prints , arXiv:2104.03719 (2021), arXiv:2104.03719 [quant-ph].
[307] C. Tang, A. Shankar, D. Meiser, D. H. E. Dubin, J. J. Bollinger, and S. E. Parker, Equilibration of the planar modes of ultracold two-dimensional ion crystals in a penning trap, Physical Review A **104**, 10.1103/physreva.104.023325 (2021).
[308] X.-Q. Li, S. Zhang, J. Zhang, W. Wu, C. Guo, and P.-X. Chen, Fast laser cooling using optimal quantum control, Physical Review A **104**, 10.1103/physreva.104.043106 (2021).
[309] J. Mielke, J. Pick, J. A. Coenders, T. Meiners, M. Niemann, J. M. Cornejo, S. Ulmer, and C. Ospelkaus, 139 GHz UV phase-locked Raman laser system for thermometry and sideband cooling of $^9Be^+$ ions in a Penning trap, Journal of Physics B Atomic Molecular Physics **54**, 195402 (2021), arXiv:2106.13532 [physics.atom-ph].
[310] D. An, A. M. Alonso, C. Matthiesen, and H. Häffner, Coupling Two Laser-Cooled Ions via a Room-Temperature Conductor, Phys. Rev. Lett. **128**, 063201 (2022), arXiv:2107.00851 [quant-ph].
[311] A. J. Rasmusson, M. D'Onofrio, Y. Xie, J. Cui, and P. Richerme, Optimized pulsed sideband cooling and enhanced thermometry of trapped ions, Physical Review A **104**, 10.1103/physreva.104.043108 (2021).
[312] W. Li, S. Wolf, L. Klein, D. Budker, C. E. Düllmann, and F. Schmidt-Kaler, Robust polarization gradient cooling of trapped ions, New Journal of Physics **24**, 043028 (2022).
[313] M. L. Cai, Z. D. Liu, Y. Jiang, Y. K. Wu, Q. X. Mei, W. D. Zhao, L. He, X. Zhang, Z. C. Zhou, and L. M. Duan, Probing a Dissipative Phase Transition with a Trapped Ion through Reservoir Engineering, Chinese Physics Letters **39**, 020502 (2022), arXiv:2202.03690 [quant-ph].
[314] W. Li, S. Wolf, L. Klein, D. Budker, C. E. Düllmann, and F. Schmidt-Kaler, Robust polarization gradient cooling of trapped ions, New Journal of Physics **24**, 043028 (2022), arXiv:2109.00575 [physics.atom-ph].
[315] J. Berrocal, E. Altozano, F. Domínguez, M. J. Gutiérrez, J. Cerrillo, F. J. Fernández, M. Block, C. Ospelkaus, and D. Rodríguez, Formation of two-ion crystals by injection from a paul-trap source into a high-magnetic-field penning trap, Physical Review A **105**, 10.1103/physreva.105.052603 (2022).
[316] F. Stopp, H. Lehec, and F. Schmidt-Kaler, A deterministic single ion fountain, Quantum Science and Technology **7**, 034002 (2022), arXiv:2108.06948 [quant-ph].
[317] R. S. Lous and R. Gerritsma, Ultracold ion-atom experiments: cooling, chemistry, and quantum effects, in *Advances In Atomic, Molecular, and Optical Physics* (Elsevier, 2022) pp. 65–133.
[318] P.-Y. Hou, J. J. Wu, S. D. Erickson, D. C. Cole, G. Zarantonello, A. D. Brandt, A. C. Wilson, D. H. Slichter, and D. Leibfried, Coherently Coupled Mechanical Oscillators in the Quantum Regime, arXiv e-prints , arXiv:2205.14841 (2022), arXiv:2205.14841 [quant-ph].
[319] D. R. Leibrandt, S. G. Porsev, C. Cheung, and M. S. Safronova, Prospects of a thousand-ion Sn^{2+} Coulomb-crystal clock with sub-10^{-19} inaccuracy, arXiv e-prints , arXiv:2205.15484 (2022), arXiv:2205.15484 [physics.atom-ph].
[320] M. Nötzold, R. Wild, C. Lochmann, and R. Wester, Spectroscopy and ion thermometry of c2- using laser-cooling transitions, Physical Review A **106**, 10.1103/physreva.106.023111 (2022).
[321] C. Lee, S. C. Webster, J. M. Toba, O. Corfield, G. Porter, and R. C. Thompson, Measurement-based ground state cooling of a trapped ion oscillator (2022).
[322] B. Efron, Bootstrap methods: Another look at the jackknife, Ann. Statist. **7**, 1 (1979).
[323] D. N. Politis and J. P. Romano, The stationary bootstrap, Journal of the American Statistical Association **89**, 1303 (1994).
[324] M. Srednicki, Entropy and area, Physical Review Letters **71**, 666 (1993).
[325] P. Calabrese and J. Cardy, Entanglement entropy and quantum field theory, Journal of Statistical Mechanics: Theory and Experiment **2004**, P06002 (2004).
[326] S. Ryu and T. Takayanagi, Holographic derivation of entanglement entropy from the anti-de sitter space/conformal field theory correspondence, Physical Review Letters **96**, 10.1103/physrevlett.96.181602 (2006).
[327] M. M. Wolf, Violation of the entropic area law for fermions, Phys. Rev. Lett. **96**, 010404 (2006).
[328] D. Gioev and I. Klich, Entanglement entropy of fermions in any dimension and the widom conjecture, Phys. Rev. Lett. **96**, 100503 (2006).
[329] S. Ryu and T. Takayanagi, Holographic derivation of entanglement entropy from the anti–de sitter space/conformal field theory correspondence, Physical Review Letters **96**, 10.1103/physrevlett.96.181602 (2006).
[330] S. Ryu and T. Takayanagi, Aspects of holographic entanglement entropy, Journal of High Energy Physics **2006**, 045 (2006).
[331] H. Casini and M. Huerta, Entanglement entropy in free quantum field theory, Journal of Physics A: Mathematical and Theoretical **42**, 504007 (2009).
[332] P. Calabrese and J. Cardy, Entanglement entropy and conformal field theory, Journal of Physics A: Mathematical and Theoretical **42**, 504005 (2009).
[333] M. B. Hastings, I. González, A. B. Kallin, and R. G. Melko, Measuring renyi entanglement entropy in quantum monte carlo simulations, Phys. Rev. Lett. **104**, 157201 (2010).
[334] B. Swingle, Constructing holographic spacetimes using entanglement renormalization, arXiv e-prints , arXiv:1209.3304 (2012), arXiv:1209.3304 [hep-th].
[335] B. Swingle, Entanglement sum rules, Physical Review Letters **111**, 10.1103/physrevlett.111.100405 (2013).
[336] B. Swingle, Interplay between short- and long-range entanglement in symmetry-protected phases, Physical Review B **90**, 10.1103/physrevb.90.035451 (2014).
[337] B. Swingle, J. McMinis, and N. M. Tubman, Oscillating terms in the renyi entropy of fermi gases and liquids, Physical Review B **87**, 10.1103/physrevb.87.235112 (2013).
[338] T. Hartman and J. Maldacena, Time evolution of entanglement entropy from black hole interiors, Journal of High Energy Physics **2013**, 10.1007/jhep05(2013)014 (2013).
[339] B. Swingle, Structure of entanglement in regulated lorentz invariant field theories (2013).
[340] B. Swingle, A simple model of many-body localization (2013).
[341] S. H. Shenker and D. Stanford, Black holes and the

butterfly effect, Journal of High Energy Physics **2014**, 10.1007/jhep03(2014)067 (2014).
[342] B. Swingle, Entanglement does not generally decrease under renormalization, Journal of Statistical Mechanics: Theory and Experiment **2014**, P10041 (2014).
[343] J. Maldacena and L. Susskind, Cool horizons for entangled black holes, Fortschritte der Physik **61**, 781 (2013).
[344] B. Swingle and M. Van Raamsdonk, Universality of Gravity from Entanglement, arXiv e-prints , arXiv:1405.2933 (2014), arXiv:1405.2933 [hep-th].
[345] B. Swingle, L. Huijse, and S. Sachdev, Entanglement entropy of compressible holographic matter: Loop corrections from bulk fermions, Phys. Rev. B **90**, 045107 (2014), arXiv:1308.3234 [hep-th].
[346] B. Swingle and I. H. Kim, Reconstructing quantum states from local data, Physical Review Letters **113**, 10.1103/physrevlett.113.260501 (2014).
[347] B. Czech, P. Hayden, N. Lashkari, and B. Swingle, The information theoretic interpretation of the length of a curve, Journal of High Energy Physics **2015**, 10.1007/jhep06(2015)157 (2015).
[348] B. Swingle and J. McGreevy, Area law for gapless states from local entanglement thermodynamics, Physical Review B **93**, 10.1103/physrevb.93.205120 (2016).
[349] D. Harlow, Jerusalem lectures on black holes and quantum information, Reviews of Modern Physics **88**, 10.1103/revmodphys.88.015002 (2016).
[350] B. Swingle, J. McGreevy, and S. Xu, Renormalization group circuits for gapless states, Physical Review B **93**, 10.1103/physrevb.93.205159 (2016).
[351] B. Swingle and J. McGreevy, Mixed s-sourcery: Building many-body states using bubbles of nothing, Physical Review B **94**, 10.1103/physrevb.94.155125 (2016).
[352] R. Mahajan, C. D. Freeman, S. Mumford, N. Tubman, and B. Swingle, Entanglement structure of non-equilibrium steady states, arXiv e-prints , arXiv:1608.05074 (2016), arXiv:1608.05074 [cond-mat.str-el].
[353] D. A. Roberts and B. Swingle, Lieb-robinson bound and the butterfly effect in quantum field theories, Physical Review Letters **117**, 10.1103/physrevlett.117.091602 (2016).
[354] A. Almheiri, X. Dong, and B. Swingle, Linearity of holographic entanglement entropy, Journal of High Energy Physics **2017**, 74 (2017), arXiv:1606.04537 [hep-th].
[355] G. Salton, B. Swingle, and M. Walter, Entanglement from topology in chern-simons theory, Physical Review D **95**, 10.1103/physrevd.95.105007 (2017).
[356] R. Islam, R. Ma, P. M. Preiss, M. Eric Tai, A. Lukin, M. Rispoli, and M. Greiner, Measuring entanglement entropy in a quantum many-body system, Nature **528**, 77 EP (2015).
[357] F. Pastawski, J. Eisert, and H. Wilming, Towards holography via quantum source-channel codes, Physical Review Letters **119**, 10.1103/physrevlett.119.020501 (2017).
[358] J. Haegeman, B. Swingle, M. Walter, J. Cotler, G. Evenbly, and V. B. Scholz, Rigorous free-fermion entanglement renormalization from wavelet theory, Physical Review X **8**, 10.1103/physrevx.8.011003 (2018).
[359] K. Li, M. Han, D. Qu, Z. Huang, G. Long, Y. Wan, D. Lu, B. Zeng, and R. Laflamme, Measuring holographic entanglement entropy on a quantum simulator, npj Quantum Information **5**, 10.1038/s41534-019-0145-z (2019).
[360] J. Cotler, P. Hayden, G. Penington, G. Salton, B. Swingle, and M. Walter, Entanglement wedge reconstruction via universal recovery channels, Physical Review X **9**, 10.1103/physrevx.9.031011 (2019).
[361] B. Grado-White and D. Marolf, Marginally trapped surfaces and AdS/CFT, Journal of High Energy Physics **2018**, 10.1007/jhep02(2018)049 (2018).
[362] S. Johri, D. S. Steiger, and M. Troyer, Entanglement spectroscopy on a quantum computer, Phys. Rev. B **96**, 195136 (2017).
[363] P. Nguyen, T. Devakul, M. G. Halbasch, M. P. Zaletel, and B. Swingle, Entanglement of purification: from spin chains to holography, Journal of High Energy Physics **2018**, 98 (2018), arXiv:1709.07424 [hep-th].
[364] G. Penington, Entanglement wedge reconstruction and the information paradox, Journal of High Energy Physics **2020**, 2 (2020), arXiv:1905.08255 [hep-th].
[365] S. Xu and B. Swingle, Accessing scrambling using matrix product operators, Nature Physics **16**, 199 (2019).
[366] S. Sahu, S. Xu, and B. Swingle, Scrambling dynamics across a thermalization-localization quantum phase transition, Physical Review Letters **123**, 10.1103/physrevlett.123.165902 (2019).
[367] S. Xu and B. Swingle, Locality, quantum fluctuations, and scrambling, Physical Review X **9**, 10.1103/physrevx.9.031048 (2019).
[368] K. Choo, C. W. von Keyserlingk, N. Regnault, and T. Neupert, Measurement of the entanglement spectrum of a symmetry-protected topological state using the ibm quantum computer, Phys. Rev. Lett. **121**, 086808 (2018).
[369] H. Gharibyan, M. Hanada, B. Swingle, and M. Tezuka, Quantum lyapunov spectrum, Journal of High Energy Physics **2019**, 10.1007/jhep04(2019)082 (2019).
[370] J. Couch, S. Eccles, T. Jacobson, and P. Nguyen, Holographic complexity and volume, Journal of High Energy Physics **2018**, 10.1007/jhep11(2018)044 (2018).
[371] S. Cooper, M. Rozali, B. Swingle, M. V. Raamsdonk, C. Waddell, and D. Wakeham, Black hole microstate cosmology, Journal of High Energy Physics **2019**, 10.1007/jhep07(2019)065 (2019).
[372] L. Cincio, Y. Subaşı, A. T. Sornborger, and P. J. Coles, Learning the quantum algorithm for state overlap, New Journal of Physics **20**, 113022 (2018).
[373] N. M. Linke, S. Johri, C. Figgatt, K. A. Landsman, A. Y. Matsuura, and C. Monroe, Measuring the rényi entropy of a two-site fermi-hubbard model on a trapped ion quantum computer, Phys. Rev. A **98**, 052334 (2018).
[374] J. Martyn and B. Swingle, Product spectrum ansatz and the simplicity of thermal states, Physical Review A **100**, 10.1103/physreva.100.032107 (2019).
[375] J. Couch, S. Eccles, P. Nguyen, B. Swingle, and S. Xu, Speed of quantum information spreading in chaotic systems, Physical Review B **102**, 10.1103/physrevb.102.045114 (2020).
[376] T. Brydges, A. Elben, P. Jurcevic, B. Vermersch, C. Maier, B. P. Lanyon, P. Zoller, R. Blatt, and C. F. Roos, Probing rényi entanglement entropy via randomized measurements, Science **364**, 260 (2019).
[377] R. Belyansky, P. Bienias, Y. A. Kharkov, A. V. Gorshkov, and B. Swingle, Minimal model for fast scrambling, Physical Review Letters **125**, 10.1103/physrevlett.125.130601 (2020).
[378] N. Klco and M. J. Savage, Systematically localizable operators for quantum simulations of quantum field theories, Physical Review A **102**, 10.1103/physreva.102.012619 (2020).
[379] C. D. White, C. Cao, and B. Swingle, Conformal field theories are magical, Physical Review B **103**, 10.1103/physrevb.103.075145 (2021).
[380] C. Zanoci and B. Swingle, Temperature-dependent energy diffusion in chaotic spin chains, Phys. Rev. B **103**, 115148 (2021), arXiv:2012.11601 [cond-mat.str-el].
[381] S.-K. Jian, C. Liu, X. Chen, B. Swingle, and P. Zhang, Quantum error as an emergent magnetic field, arXiv e-prints , arXiv:2106.09635 (2021), arXiv:2106.09635 [quant-ph].
[382] S. Antonini and B. Swingle, Holographic boundary states and dimensionally reduced braneworld spacetimes, Physical Review D **104**, 10.1103/physrevd.104.046023 (2021).
[383] S. Sahu, S.-K. Jian, G. Bentsen, and B. Swingle, Entanglement Phases in large-N hybrid Brownian circuits with long-range couplings, arXiv e-prints , arXiv:2109.00013 (2021), arXiv:2109.00013 [quant-ph].
[384] S.-K. Jian and B. Swingle, Phase transition in von Neumann entanglement entropy from replica symmetry breaking, arXiv e-prints , arXiv:2108.11973 (2021), arXiv:2108.11973 [quant-ph].
[385] S.-K. Jian, C. Liu, X. Chen, B. Swingle, and P. Zhang, Measurement-induced phase transition in the monitored sachdev-ye-kitaev model, Physical Review Letters **127**, 10.1103/physrevlett.127.140601 (2021).
[386] S.-K. Jian and B. Swingle, Chaos-protected locality, Journal of High Energy Physics **2022**, 10.1007/jhep01(2022)083 (2022).
[387] S. Xu and B. Swingle, Scrambling Dynamics and Out-of-Time Ordered Correlators in Quantum Many-Body Systems: a Tutorial, arXiv e-prints , arXiv:2202.07060 (2022), arXiv:2202.07060 [quant-ph].
[388] N. Klco, A. Roggero, and M. J. Savage, Standard model physics and the digital quantum revolution: thoughts about the interface, Reports on Progress in Physics **85**, 064301 (2022).
[389] S. Sahu and B. Swingle, Efficient tensor network simulation of quantum many-body physics on sparse graphs, arXiv e-prints , arXiv:2206.04701 (2022), arXiv:2206.04701 [quant-ph].
[390] J. Preskill, Quantum information notes: Foundations of quantum theory ii: Measurement and evolution, October, 2018 ().
[391] Andrew Shaw, Benchmarking Lattice Gauge Theories With NISQ Algorithms (2020).
[392] H. D. Zeh, On the interpretation of measurement in quantum theory, Foundations of Physics **1**, 69 (1970).
[393] K. L. Hur, Entanglement entropy, decoherence, and quantum phase transitions of a dissipative two-level system, Annals of Physics **323**, 2208 (2008).
[394] Z. Xu, L. P. Garcí a-Pintos, A. Chenu, and A. del Campo, Extreme decoherence and quantum chaos, Physical Review Letters **122**, 10.1103/physrevlett.122.014103 (2019).
[395] C. Zanoci and B. Swingle, Entanglement and thermalization in

open fermion systems (2016).
[396] A. del Campo and T. Takayanagi, Decoherence in conformal field theory, Journal of High Energy Physics **2020**, 10.1007/jhep02(2020)170 (2020).
[397] S.-K. Jian and B. Swingle, Note on entropy dynamics in the brownian SYK model, Journal of High Energy Physics **2021**, 10.1007/jhep03(2021)042 (2021).
[398] J. Couch, S. Eccles, P. Nguyen, B. Swingle, and S. Xu, Speed of quantum information spreading in chaotic systems, Phys. Rev. B **102**, 045114 (2020).
[399] G. Bacciagaluppi, The Role of Decoherence in Quantum Mechanics, The Stanford Encyclopedia of Philosophy (2020).
[400] S. Mancini, H. Moya-Cessa, and P. Tombesi, Vibrational superposition states without rotating wave approximation, Journal of Modern Optics **47**, 2133 (2000).
[401] H.-S. Zeng, L.-M. Kuang, and K.-L. Gao, Jaynes-cummings model dynamics in two trapped ions (2001).
[402] O. E. Müstecaplıoğlu and L. You, Motional rotating wave approximation for harmonically trapped particles (2001).
[403] M. Feng, Series solution to the laser-ion interaction in a raman-type configuration, The European Physical Journal D - Atomic, Molecular and Optical Physics **18**, 371 (2002).
[404] L. M. A. Aguilar and H. Moya-Cessa, Generalized qubits of the vibrational motion of a trapped ion, Physical Review A **65**, 10.1103/physreva.65.053413 (2002).
[405] P. Aniello, V. Man'ko, G. Marmo, A. Porzio, S. Solimeno, and F. Zaccaria, Trapped ions interacting with laser fields: a perturbative analysis without rotating wave approximation (2003).
[406] P. Aniello, A. Porzio, and S. Solimeno, Evolution of the jaynes-cummings model beyond the standard rotating wave approximation, Journal of Optics B: Quantum and Semiclassical Optics **5**, S233 (2003).
[407] T. Liu, K. L. Wang, and M. Feng, Lower ground state due to counter-rotating wave interaction in a trapped ion system, Journal of Physics B: Atomic, Molecular and Optical Physics **40**, 1967 (2007).
[408] D. Wang, T. Hansson, A. Larson, H. O. Karlsson, and J. Larson, Quantum interference structures in trapped-ion dynamics beyond the lamb-dicke and rotating wave approximations, Physical Review A **77**, 10.1103/physreva.77.053808 (2008).
[409] K. Park, J. Hastrup, P. Marek, U. L. Andersen, and R. Filip, Quantum rabi interferometry of motion and radiation (2022).
[410] J. Venkatraman, X. Xiao, R. G. Cortiñas, and M. H. Devoret, On the static effective lindbladian of the squeezed kerr oscillator (2022).
[411] W. E. Lamb, A note on the capture of slow neutrons in hydrogenous substances, Phys. Rev. **51**, 187 (1937).
[412] R. H. Dicke, The effect of collisions upon the doppler width of spectral lines, Phys. Rev. **89**, 472 (1953).
[413] L. F. Wei, Y.-x. Liu, and F. Nori, Engineering quantum pure states of a trapped cold ion beyond the lamb-dicke limit, Phys. Rev. A **70**, 063801 (2004).
[414] R. Dermez, Quantifying of quantum entanglement in Schrödinger cat states with the trapped ion-coherent system for the deep Lamb-Dick regime, Indian Journal of Physics **95**, 219 (2021).
[415] A.-H. Abdel-Aty, A. B. A. Mohamed, and H. Eleuch, Nonlocality Dynamics Induced by a Lamb-Dicke Nonlinearity in Two Dipole-Coupled Trapped Ions Under Intrinsic Decoherence, Fractals **30**, 2240045-1988 (2022).
[416] M. Kang, Q. Liang, M. Li, and Y. Nam, Efficient motional-mode characterization for high-fidelity trapped-ion quantum computing (2022).
[417] W. Magnus, On the exponential solution of differential equations for a linear operator, Communications on Pure and Applied Mathematics **7**, 649 (1954).
[418] N. Goldman and J. Dalibard, Periodically driven quantum systems: Effective hamiltonians and engineered gauge fields, Phys. Rev. X **4**, 031027 (2014).
[419] T. Nag, D. Sen, and A. Dutta, Maximum group velocity in a one-dimensional model with a sinusoidally varying staggered potential, Phys. Rev. A **91**, 063607 (2015).
[420] T. Kuwahara, T. Mori, and K. Saito, Floquet-magnus theory and generic transient dynamics in periodically driven many-body quantum systems, Annals of Physics **367**, 96 (2016).
[421] A. D'Arrigo, G. Falci, and E. Paladino, High-fidelity two-qubit gates via dynamical decoupling of local $1/f$ noise at the optimal point, Phys. Rev. A **94**, 022303 (2016).
[422] A. Verdeny, J. Puig, and F. Mintert, Quasi-periodically driven quantum systems, Zeitschrift für Naturforschung A **71**, 897 (01 Oct. 2016).
[423] B. Zhu, T. Rexin, and L. Mathey, Magnus expansion approach to parametric oscillator systems in a thermal bath, Zeitschrift für Naturforschung A **71**, https://doi.org/10.1515/zna-2016-0135 (01 Oct. 2016).
[424] C. D. Parmee and N. R. Cooper, Stable collective dynamics of two-level systems coupled by dipole interactions, Phys. Rev. A **95**, 033631 (2017).
[425] T. Shirai, T. Mori, and S. Miyashita, Floquet–gibbs state in open quantum systems, The European Physical Journal Special Topics **227**, 323 (2018).
[426] A. Iserles, K. Kropielnicka, and P. Singh, Magnus-Lanczos methods with simplified commutators for the Schrödinger equation with a time-dependent potential, arXiv e-prints , arXiv:1801.06913 (2018), arXiv:1801.06913 [math.NA].
[427] P. Nalbach and V. Leyton, Magnus expansion for a chirped quantum two-level system, Phys. Rev. A **98**, 023855 (2018).
[428] T. Haga, Divergence of the floquet-magnus expansion in a periodically driven one-body system with energy localization, Phys. Rev. E **100**, 062138 (2019).
[429] A. Haldar, D. Sen, R. Moessner, and A. Das, Scars in strongly driven Floquet matter: resonance vs emergent conservation laws, arXiv e-prints , arXiv:1909.04064 (2019), arXiv:1909.04064 [cond-mat.other].
[430] D. Zeuch, F. Hassler, J. Slim, and D. P. DiVincenzo, Exact Rotating Wave Approximation, arXiv e-prints , arXiv:1807.02858 (2018), arXiv:1807.02858 [quant-ph].
[431] J. C. Halimeh and P. Hauke, Origin of staircase prethermalization in lattice gauge theories, arXiv e-prints , arXiv:2004.07254 (2020), arXiv:2004.07254 [cond-mat.str-el].
[432] Á. Gómez-León and G. Platero, Designing adiabatic time-evolution from high frequency bichromatic sources, arXiv e-prints , arXiv:2008.10750 (2020), arXiv:2008.10750 [cond-mat.mes-hall].
[433] D. Zeuch and D. P. DiVincenzo, Refuting a Proposed Axiom for Defining the Exact Rotating Wave Approximation, arXiv e-prints , arXiv:2010.02751 (2020), arXiv:2010.02751 [quant-ph].
[434] Z. Davoudi, M. Hafezi, C. Monroe, G. Pagano, A. Seif, and A. Shaw, Towards analog quantum simulations of lattice gauge theories with trapped ions, Physical Review Research **2**, 023015 (2020), arXiv:1908.03210 [quant-ph].
[435] Z. Davoudi, N. M. Linke, and G. Pagano, Toward simulating quantum field theories with controlled phonon-ion dynamics: A hybrid analog-digital approach, Physical Review Research **3**, 043072 (2021), arXiv:2104.09346 [quant-ph].
[436] B. Andrade, Z. Davoudi, T. Graß, M. Hafezi, G. Pagano, and A. Seif, Engineering an effective three-spin hamiltonian in trapped-ion systems for applications in quantum simulation, Quantum Science and Technology **7**, 034001 (2022).
[437] G. Martín-Vázquez, G. Aarts, M. Müller, and A. Bermudez, Long-range ising interactions mediated by $\lambda\phi^4$ fields: Probing the renormalization of sound in crystals of trapped ions, PRX Quantum **3**, 020352 (2022).
[438] E. Chertkov, J. Bohnet, D. Francois, J. Gaebler, D. Gresh, A. Hankin, K. Lee, D. Hayes, B. Neyenhuis, R. Stutz, A. C. Potter, and M. Foss-Feig, Holographic dynamics simulations with a trapped-ion quantum computer, Nature Physics **18**, 1074 (2022).
[439] O. Katz and C. Monroe, Programmable quantum simulations of bosonic systems with trapped ions (2022).
[440] L.-L. Yan, L.-Y. Wang, S.-L. Su, F. Zhou, and M. Feng, Verification of information thermodynamics in a trapped ion system, Entropy **24**, 10.3390/e24060813 (2022).
[441] B. W. Li, Q. X. Mei, Y. K. Wu, M. L. Cai, Y. Wang, L. Yao, Z. C. Zhou, and L. M. Duan, Observation of non-markovian spin dynamics in a jaynes-cummings-hubbard model using a trapped-ion quantum simulator (2022).
[442] M. Meth, V. Kuzmin, R. van Bijnen, L. Postler, R. Stricker, R. Blatt, M. Ringbauer, T. Monz, P. Silvi, and P. Schindler, Probing phases of quantum matter with an ion-trap tensor-network quantum eigensolver (2022).
[443] D. Lewis, L. Banchi, Y. H. Teoh, R. Islam, and S. Bose, Ion Trap Long-Range XY Model for Quantum State Transfer and Optimal Spatial Search, arXiv e-prints , arXiv:2206.13685 (2022), arXiv:2206.13685 [quant-ph].
[444] Andrew Shaw, Towards Analog Quantum Simulation of Lattice Gauge Theories (2020).
[445] O. Katz, M. Cetina, and C. Monroe, Programmable n-body interactions with trapped ions (2022).
[446] O. Katz, L. Feng, A. Risinger, C. Monroe, and M. Cetina, Demonstration of three- and four-body interactions between trapped-ion spins (2022).
[447] V. M. Bastidas, T. Haug, C. Gravel, L.-C. Kwek, W. J. Munro, and K. Nemoto, Stroboscopic hamiltonian engineering in the low-frequency regime with a one-dimensional quantum processor, Physical Review B **105**, 10.1103/physrevb.105.075140 (2022).
[448] Andrew Shaw, Benchmarking quantum simulators (2021).